A Quantum Kuramoto Model

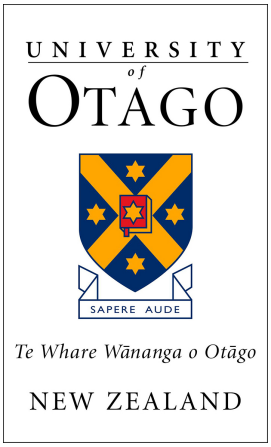

Malcolm E. K. Morrison

Department of Physics, University of Otago
Supervisor: Dr. Ashton Bradley

A dissertation submitted in partial fulfillment of the requirements for the degree of BSc(Hons) in Physics, University of Otago, 2013.

Abstract

The Kuramoto model is the most studied and comprehensive framework of classical synchronization. It describes a large number of weakly coupled oscillators with a phase transition between synchronized and incoherent states at a critical coupling strength. We construct a quantum Hamiltonian that collapses to the Kuramoto model in the appropriate limit. Using the truncated Wigner formulation we analyze the behaviour of this system and its classical limit. We find that with both number and coherent initial states only transient synchronization is possible. However, when comparing the systems where this transient synchronization can occur with synchronization in the classical model we find that the critical coupling strengths match for both systems.

Acknowledgments

Firstly I would like to thank the ever enthusiastic Ashton Bradley for being such a great supervisor to have. Thank you for having the patience to explain to me much of the content that I would often try to teach myself and inevitably form wrong ideas about. Many times when showing you results that I had spent hours staring at, having existential crises over, you would become very excited and put me back on track. It was a pleasure working under your supervision.

Secondly I would like to thank my fellow honours students for not murdering me in my sleep. I know that I can be very excitable, noisy, attention demanding and at times downright annoying. So thank you all for putting up with me and I apologize for all of the times that I have distracted you all from your work. You are all a great bunch of people and I wish you the best in whatever you choose to do.

Finally I would like to thank all of the people in the Physics department at the University of Otago. everyone is so supportive and I couldn't dream up a friendlier environment to work and learn in.

Contents

Chapter 1

Introduction

Synchronization is a phenomenon that describes objects with a periodic motion locking in phase with one another. It is an emergent phenomenon of spontaneous order in a universe where things tend towards disorder. A surprising number of things in our lives are governed by this phenomenon, ranging from our own circadian rythm[1] to laser beams[2].

A canonical model of synchronization is the Kuramoto model, which deals with similar, weakly sinusoidally coupled oscillators.

There is currently a lot of interest in quantum synchronization. It has recently become possible to construct nano-scale, mechanical oscillators that are governed by the laws of quantum mechanics[3]. In the last few weeks there have been a couple of papers released that cover dissipative quantum Kuramoto synchronization[4] and measures of synchronization[5] respectively. As the Kuramoto model is such a well understood canonical model of classical synchronization, we ask whether or not there exists a quantum analogy to it.

In this thesis I will take you on a journey through the history of synchronization, eventually constructing and exploring a fully quantum Kuramoto model. This will be broken up into several chapters that will cover different material.

The background chapter will cover several of the important studies in the history of sync and eventually cover the Kuramoto model itself. I have covered the history in such a way as to slowly introduce, and make you comfortable with the key features of synchronization so that I may later compare them with my results.

In the last section I will talk in more detail about the motivation and aims of my project.

Chapter 3 will cover the background theory that I had to use in order to complete this project. This includes quantum mechanics and phase space formalism. The final section will cover common examples of initial states that I will use in chapter 5

The numerical methods are covered in chapter 4. Here I will describe what sacrifices that I made in order to be able to utilize my computational resources efficiently.

In the results chapter I will present my findings in two sections again. Firstly I will look at the classical limit, show that it is analogous to the Kuramoto model and simulate the dynamics. This was done because the majority of work that I have read

in the field is done in the classical limits of their respective models, so this will provide a useful comparison. Then I will simulate the full quantum behaviour of my system and go through the results of that.

Chapter 2

Background

In this chapter I will cover the history of synchronization as a field of research up until the Kuramoto model. Section 2.1 is heavily drawn from the book Sync [2] and then section 2.2 is based on reference [6] both of which are by Steven Strogatz.

2.1 The History of Sync

In the year 1915 a fierce debate started in the scientific community over the fireflies of Southeast Asia. For over 300 years western travelers had been returning from there with stories of thousands of fireflies flashing in unison, lighting up whole sections of a riverbank or forest at a time. But it was only in the early twentieth century that a fully fledged investigation began.

Figure 2.1: Fireflies use their bioluminescence to attract mates through a series of flashes.[7]

What springs to mind when one thinks about synchronized behavior are things like musicians playing in time with the beat, dancers keeping in step and various other things with one crucial link: intelligence. For intelligent humans synchronous behaviour is almost second nature, but we still have to consciously try to achieve it. For this reason one might think that synchronization is a phenomenon that requires intelligence and yet these simple, "unintelligent" insects were managing to pull it off. You can see why scientists around the world were arguing over this for decades, as Philip Laurent summed up so nicely for the 1917 issue of *Science*; "I could hardly believe my eyes, for such a thing to occur among insects is certainly contrary to all natural laws."

As the century progressed the sheer number of systems that behave in a synchronized manner became apparent, each raising more questions. Why do yeast cell suspensions metabolically synchronize[1]? How do menstrual periods sync up in women[1]? How is it that tiny cells connected together, each with oscillating electric potentials, work together to create brain waves and conscious thought[1, 8]? What was even more baffling to the scientists involved was that some cases were found in non-living systems. The first study of non-living synchronization goes all the way back to the year 1665[2].

2.1.1 Huygens Pendulum Clocks

Christiaan Huygens was a Dutch physicist and inventor of the pendulum clock. Pairs of these clocks were taken aboard ships so that they could accurately measure the ship's current longitude by comparing the time from a known longitude with the local midday. They took pairs so that if one failed, there would be a back up, but this had an interesting side effect. Huygens himself noticed that: "...these two clocks hanging next to one another separated by one or two feet keep an agreement so exact that the pendulums always oscillate together without variation."[2]

To determine the cause of this synchronization Huygens performed a series of experiments and found the results to be surprising. The clocks would only synchronize when sufficiently close and similarly oriented, so there must have been some local interaction between the pendulums. He then hung the clocks from a board supported by two chairs. When he disrupted the pendulums from their synchronized state the chairs stated shaking and would continue to do so until the clocks had re-synchronized. From this he concluded that the pendulums moving made the clocks wobble slightly, causing the wooden planks to jiggle, shaking the chairs. But when the clocks were perfectly anti-synchronized the forces canceled and thus the chairs were still. This formed what is called a negative feedback loop: if one of the pendulums desynchronizes slightly, then the forces will become unbalanced in such a way that the pendulum is knocked back into perfect anti-sync.

Huygens had discovered non-living sync. He had shown, without realizing its significance at the time, that things do not have to be living to have synchronous behaviour, flying in the face of many twentieth century ideas. Discoveries like this eventually swayed the opinions of the scientific community to see sync in a new light: intelligence was not required at all! In fact, it seemed as though very simple systems could exhibit synchronous behaviour. This and the numerous applications in health-care and biology prompted some to start making theoretical models of this phenomenon.

2.1.2 Modeling Sync

One of the first to model sync was Charlie Paskin[9], applied mathematician at New York University's Courant Institute. In 1975 Peskin was already well known for his detailed analysis of three-dimensional blood flow patterns in the heart when he decided to turn his attention to the heart's pacemaker.

The pacemaker is a collection of about 10,000 cells that controls the beat of the heart. It is an amazing example of how evolution can produce unorthodox, but immensely robust structures. Where an engineer may create a single device to maintain a pace, perhaps with a backup, our pacemakers are democratic systems of thousands of cells that collectively set a pace. They are so good at this that they manage to

beat together reliably for the entire span of our life, all three-something billion beats of it, and they do all of this without any oversight from the brain. Peskin posed similar question to those before him: How do these cells, with no leader or outside instructions, manage to get in sync?

To investigate this he modeled each cell as an identical capacitor in parallel with a resistor. The charge would build up on the capacitor at a decreasing rate, due to the resistor, until it reaches a threshold voltage when it would discharge to repeat the process again (figure 2.2). He then took the cardiac pacemaker to be a collection of these cells that would only interact when the capacitor discharged. Those close to discharging would be kicked closer to it. Those further away from discharging would be knocked further away.

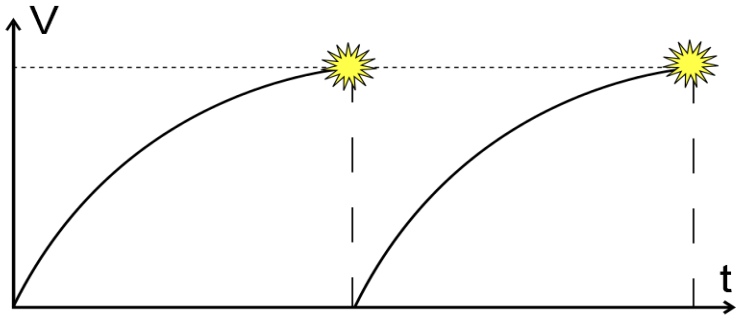

Figure 2.2: The voltage across the Paskin's cells increased like an RC circuit until a threshold voltage is reached. The cell then fires, nudging up the voltage across other cells while returning back to zero. This repeats *ad infinitum*.

Straight away you can see that this is a tricky system to analyze, especially when all of the capacitors are at different points in this cycle. However, Paskin persisted and conjectured that this system would always synchronize, no matter how it was initially started. That is, eventually and inevitably all of the cells would discharge in unison, *ad infinitum*.

This was proved 15 years later for a more general system[10]. The proof applies to any system whose "readiness to fire" - analogous to the voltage across the capacitor - builds up slower the closer it is to fire, i.e., the second derivative with respect to time is negative. The proof is also only for systems where cells[1] only knock other cell's readiness up, not down.

This analysis was a huge landmark for synchronization, proving that many biological systems did indeed synchronize, and in fact had to synchronize. This result attracted the attention of many scientists in various fields such as in neurobiology and geology

[1]Here we are talking about a cell as a general pulse coupled oscillator, not necessarily a biological cell.

because pulse-coupled oscillators described their systems more accurately than older models. However the analysis was a general proof and didn't describe the dynamics of any one system, only the end result. Further work was required.

A more qualitative approach was taken in the 1950s by one Norbert Wiener, an MIT professor in mathematics, while looking into brain waves[11]. Individual brain cells have an oscillating potential difference across them, but are imprecise and inconsistent when it comes to maintaining a steady pace. Yet when many are grouped together, like in the brain, one can detect a very consistent sinusoidal oscillation across the entire system. These are called brain waves and they come in different frequencies. Weiner was interested in alpha waves that oscillate at about 10Hz - associated with a relaxed conscious brain.

He argued that, like any biological population, brain cells are diverse and that there would be a Gaussian distribution (bell curve) of frequencies ranging from, say 8Hz to 12Hz with the majority in the center at 10Hz. If these cells had the ability to "pull" the frequencies of other cells towards them then they would spontaneously synchronize. He continued to say that if the distribution was too large, then the cells near the 10Hz center would be pulled inwards but the ones on the outskirts would not be as they are too dissimilar from the developing mass in the middle. Thus if one was to graph the resulting distribution there would be a large peak in the center with two side fringes. He concluded that this would be a good way to determine whether or not a system was governed by synchronization. This description proved true and was demonstrated numerically in 1967 by Art Winfree, a senior engineering physics student at Cornell[12].

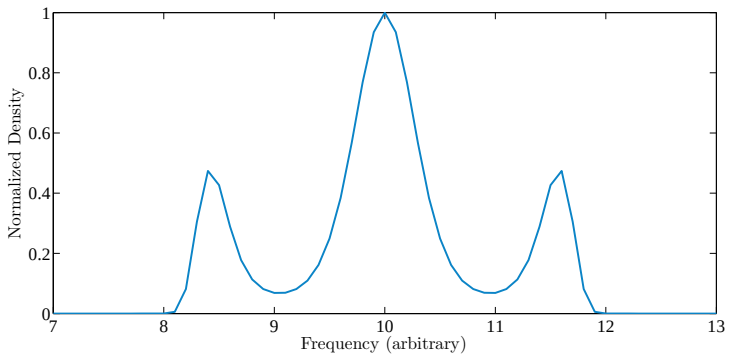

Figure 2.3: Weiner's pulling pattern. He predicted that any partially synchronized system would display a similar shape to this one.

Winfree decided to consider a system general enough to apply to any population of oscillators. He considered a large group of oscillators, each with their own natural frequency and with both a level of pulling influence dependent on the stage of its cycle,

or phase, and a level of sensitivity also dependent on its phase. Both of these functions are very general and can be positive or negative to cover the full range of dynamics. In the fireflies' case, the influence function is a single pulse per cycle. However for Huygens' clocks, these two functions would combine such as to make the phases repulsive unless anti-synchronized.

Then Winfree had to make a few approximations in order to make this problem approachable. The first of which is that that all of the oscillators were identical in all but natural frequency. That is, all of their influence and sensitivity functions are identical. Secondly, he assumed that all oscillators were connected weakly and equally to every other oscillator in the system. So with the fireflies again, each firefly can see every other firefly's flash equally. The closer ones don't have any more or any less influence than those far away.

This does make the model no longer an exact representation of many systems, for example neurons have a limited number of connections, but it does simplify the mathematics immensely without sacrificing much of the actual dynamics of the system. While fireflies do see closer flashes as being brighter, when there are thousands of them we can neglect the few that are close as most of the influence would come from the distant masses. Like an audience clapping at a concert; if there are thousands of people clapping your neighbors will be drowned out by the masses.

Mathematically, for N oscillators, this is written as:

$$\dot{\theta}_i = \omega_i + \Big(\sum_{j=1}^{N} X(\theta_j) \Big) Z(\theta_i), \quad i = 1, ..., N \tag{2.1}$$

where θ_i is the phase of the ith oscillator, ω_i its natural frequency and $Z(\theta_i)$ and $X(\theta_i)$ are the sensitivity and influence functions respectively. The dot denotes the derivative with respect to time and N is assumed to be a large number.

Several interesting things come from his analysis. Looking first at the case where the oscillators are non-interacting, the second term vanishes and each oscillator evolves at its own pace. This is what we call an incoherent system: a blur of fireflies' flashes or a crowd's applause. Winfree discovered that the system tended toward this incoherent state for some combinations of functions. Even when started in a perfectly synchronized state the system would become incoherent. Other combinations, however, led to the system to spontaneously synchronize no matter the initial state. An incoherent mass of oscillators would end up clumped together in some manner.

In the cases where the oscillators did synchronize it would start with just a few grouping together by chance. Then their cooperative influence becomes more dominant than the incoherent mass, pulling a few more nearby oscillators into the fold. This would continue until all but those with too extreme natural frequencies were assimilated into

the synchronized blob, resulting in a peak in frequencies with two side bands. This was just as Weiner predicted.

However his most important discovery was found when looking at combinations of X and Z that allowed for sync to occur. What Winfree found was that if he made the distribution of natural frequencies even a tiny bit too large, then the system would spontaneously become incoherent. He had found a very discrete phase transition between synchronization and incoherence. As the distribution is decreased in size the state will remain incoherent until a critical value is reached when suddenly oscillators will lock together in synchrony.

This is a temporal analogy to a phase transition, say, in water, when cooling it down. At a critical temperature the state changes from water to ice, in this case the melting point. When slightly above this temperature it is a liquid with molecules bouncing around but as soon as you pass this critical temperature all of the molecules snap together into an ordered state. For us the oscillators snap from a disordered, incoherent state into a synchronized, ordered state as the distribution becomes narrower than the critical value. This is a temporal analogy because instead of lining up in space, like the ice, they line up in time.

2.2 The Kuramoto Model

It was in 1975 that Yoshiki Kuramoto discovered Winfree's work and would spend the next few decades developing it further. He managed to show that for any system of similar, weakly coupled oscillators in their limit cycles, the interactions could be described by a single function of the relative phases between them. This instantly simplifies the system by combining the sensitivity and influence functions into a single function of a single variable. With this, the equations in 2.1 become:

$$\dot{\theta}_i = \omega_i + \sum_{j=1}^{N} \Gamma_{ij}(\theta_j - \theta_i), \quad i = 1, ..., N \tag{2.2}$$

where Γ_{ij} is a general function for the interaction between the ith and jth oscillators. This is still too general to extract useful dynamics from as the type of connections between oscillators are unspecified. To obtain some tangible, applicable results Kuramoto then took a page out of Winfree's book. He decided to look at the mean field case with equally weighted all-to-all coupling. The Kuramoto model is the simplest possible case where the coupling is a sine function. That is:

$$\Gamma_{ij}(\theta_j - \theta_i) = \frac{K}{N} \sin(\theta_j - \theta_i), \quad i = 1, ..., N \tag{2.3}$$

The Kuramoto model can then be written as:

$$\dot{\theta}_i = \omega_i + \frac{K}{N}\sum_{j=1}^{N}\sin(\theta_j - \theta_i), \quad i = 1, ..., N \tag{2.4}$$

where $K \geq 0$ is the coupling strength and we divide by the number of oscillators, N, so that in the $N \to \infty$ limit the system is well behaved. The frequencies are distributed by some probability density $g(\omega)$ that Kuramoto assumed to be symmetric about a mean frequency Ω, i.e. $g(\Omega + \omega) = g(\Omega - \omega)$ for any ω.

For simplicity's sake we can redefine $\theta_i \mapsto \theta_i + \Omega t$ which yields the same set of coupled differential equations 2.4, but with $g(\omega)$ now an even function, centered about 0. This corresponds to switching to a rotating frame and can be done because of the rotational symmetry in the system. Even functions are those with the property that, for any ω, $g(\omega) = g(-\omega)$ and includes Gaussian or Lorentzian distributions, which will be the most commonly used distributions in this thesis[2].

2.2.1 Order Parameter

To clearly and simply describe the behaviour of thousands upon thousands of oscillators Kuramoto introduced a complex order parameter.

If we project this system onto the complex unit circle, then all of the oscillators become points running around this circle at different speeds. With this one can easily read off the phase of any individual oscillator by merely looking at its position on the circle at any one instant. When the system is incoherent, all that we would see is a mass of dots flying around the circle with an approximately even distribution. Conversely when the system is in perfect sync we would see all of the dots rotating as a single point on the circle. Kuramoto, in an intuitive step, summed these projections to gain a description of the overall behaviour.

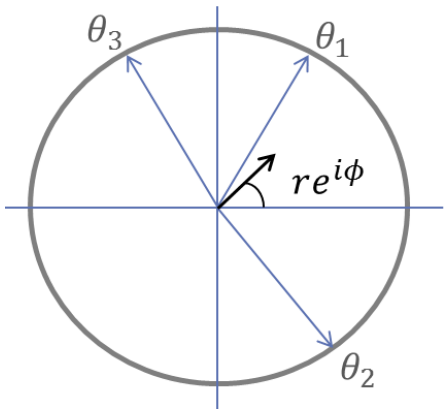

Figure 2.4: A depiction of the order parameter for three oscillators.

$$re^{i\psi} = \frac{1}{N}\sum_{j=1}^{N} e^{i\theta_j} \tag{2.5}$$

[2]The only other distribution used will be a uniform distribution. This shall be used for the phase of oscillators in order to create incoherent initial states.

Here we sum over the complex phases of each oscillator and normalize to obtain the mean phase, ψ, and the phase coherence or order parameter, $r \in [0, 1]$. It is easy to see that in the synchronized state, with all the dots on a single point, ψ will be the same as the phase of any individual oscillators and r will be exactly one. When all of the oscillators are evenly distributed around the circle r will be exactly zero. Because the incoherent system is constantly fluctuating very closely to this even distribution, the order parameter will be fluctuating between zero and some small number much less than one when in this state. Thus, r can be viewed as a measure of how ordered the system is, hence the name.

Kuramoto's next step was to rewrite his model in terms of this order parameter. Multiplying both sides of equation 2.5 with $e^{-i\theta_i}$ we obtain

$$re^{i(\psi-\theta_i)} = \frac{1}{N}\sum_{j=1}^{N} e^{i(\theta_j-\theta_i)} \tag{2.6}$$

Equating the imaginary parts yeilds

$$r\sin(\psi-\theta_i) = \frac{1}{N}\sum_{j=1}^{N} \sin(\theta_j-\theta_i) \tag{2.7}$$

Then we substituting this into 2.4 to get what we are after:

$$\dot{\theta}_i = \omega_i + Kr\sin(\psi-\theta_i), \quad i = 1, ..., N \tag{2.8}$$

It is easy to see the mean field character of the Kuramoto model when written in this form. All of the originally coupled differential equations become coupled only to the mean field quantites r and ψ, and hence the system is drastically simpler.

All of the qualitative behavior discussed in section 2.1.2 can now be seen in equation 2.8. A key point is that the effective coupling strength is proportional to the order parameter. So if the state starts with an uniform phase distribution then, initially, there is no effective coupling at all. Then the distribution in natural frequencies will cause some fluctuation in r and suddenly all of the other oscillators are slightly attracted to this mean. This creates a positive feedback loop as the effective coupling grows when more of the oscillators are drawn towards the mean phase, thus drawing them in faster and faster. This will happen until all of the oscillators that can synchronize for a given coupling strength have synchronized. The order parameter, r, will have stabilized at some constant value, r_∞, with some small fluctuations. There still might be some oscillators that cannot synchronize because of their extreme natural frequencies as described earlier.

Numerical simulations show that every combination of coupling strength with some

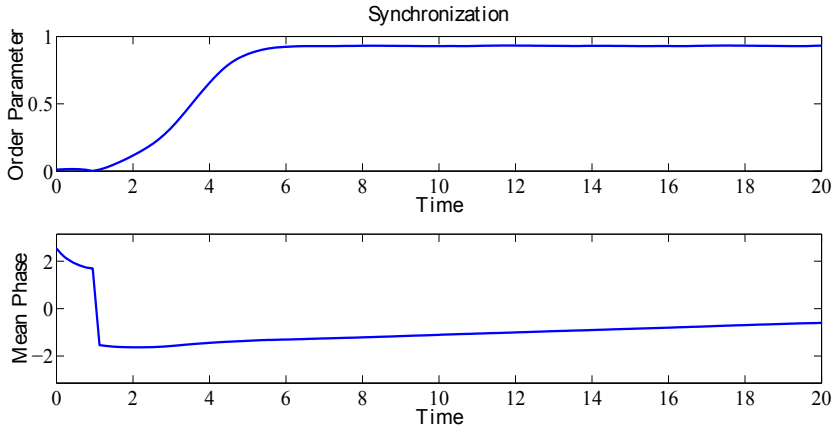

Figure 2.5: An incoherent initial state will spontaneously synchronize if the coupling strength, K, is large enough. In this case $K = 3$ with $\Delta\omega = 1$ for 10,000 oscillators

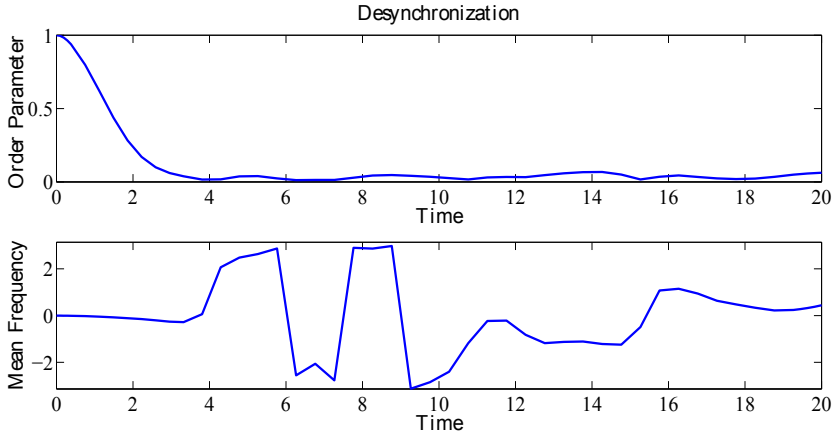

Figure 2.6: The system will spontaneously desynchronize if K is too low. Here you can see the system starts with all oscillators having the same phase, but then the system quickly becomes incoherent. This happens because $K = 0.4K_c$ for $\Delta\omega = 1$. There are 10,000 oscillators in this simulation.

distribution of frequencies has a unique value for r_∞. For K less than a critical value for the specific distribution, K_c, the system will end up incoherent. That is, $r_\infty \approx 0$. For $K > K_c$, the incoherent state is no longer stable and the system at least partially synchronizes with $r_\infty > 0$. This is an alternate form of the phase transition discussed in section 2.1.2.

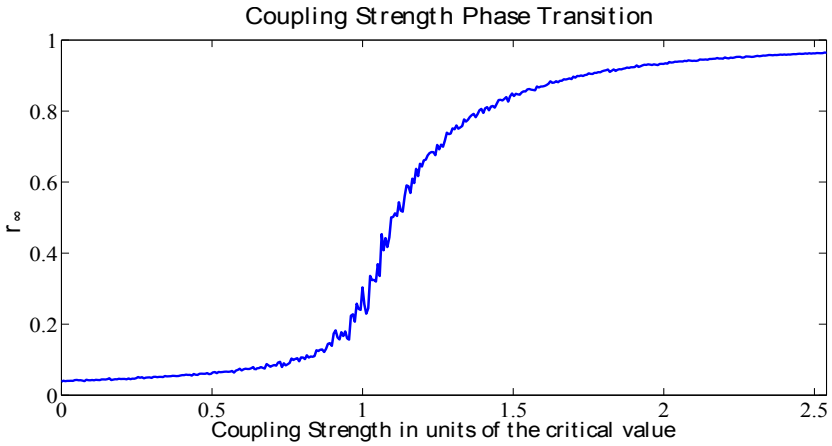

Figure 2.7: The phase transition between incoherent and synchronized. Once K is beyond the critical value the system synchronizes in part and r_∞ tends towards 1.

2.2.2 Solutions of the Kuramoto Model

The Kuramoto model reproduces the results of both Winfree and Wiener's theories: the pulling patterns in a partially synchronized state and the phase transition. But what makes it stand out as a powerful tool is that it is exactly solvable. To emphasize how amazing this is, remember that this is a huge, potentially infinite set of non-linear coupled differential equations. But still there are exact solutions for both K_c and $r_\infty(K)$. Stable solutions for r are given implicitly by[6]:

$$r = Kr \int_{-\pi/2}^{\pi} \cos^2(\theta)\, g\big(Kr\sin(\theta)\big) d\theta \tag{2.9}$$

The trivial solution of $r = 0$ is the incoherent state. This applies even for all K, but is unstable when $K > K_c$ when the system bifurcates. So, we can find the explicit value for K_c by taking the limit of $r \to 0$ from above. This gives

$$K_c = \frac{2}{\pi g(0)} \tag{2.10}$$

The value of the $r > 0$ branch can be approximately gained by expanding the integrand in equation 2.9 in a power series. Doing this we find that the bifurcation is supercritical only when $g''(0) > 0$ and subcritical when $g''(0) < 0$. This means that the $r > 0$ branch is only stable if the distribution g has a negative second derivative at $\omega = 0$, like all smooth, unimodal, even densities, such as Gaussian and Lorentzian distributions.

Taking the second order expansion of the integral in (2.9) we find that r_∞ initially scales like a square root. So just above K_c,

$$r_\infty(K) \approx \sqrt{\frac{16\,(K - K_c)}{-\pi\, K_c^4\, g''(0)}} \tag{2.11}$$

Equation 2.9 can be solved exactly for some probability distributions. Kuramoto solved this for a Lorentzian distribution and found that:

$$r_\infty(K) = \sqrt{1 - \frac{K_c}{K}} \tag{2.12}$$

for all $K \geq K_c$.

Note that equation(2.9) is not exactly solvable for Gaussian distributions, but they will be what is used throughout this thesis for reasons discussed in A.1 However they yield similar dynamics as Lorentzians.

2.3 Motivation for a Quantum Model

The Kuramoto model and related research has led to a deeper understanding of many different systems in our world ranging from earthquakes to the brain. As synchronization becomes more and more understood technologies that either harness or deal with these phenomena can be developed to a much higher level. These can include timekeeping devices, communications and power networks and even medical technologies and processes. A simple, and yet life changing example has been treating circadian desynchronization in blind people. Eighty percent of blind people are not effected by the synchronizing effect that the sun has on us and therefore find it very challenging to keep a sleep cycle like the rest of us[2]. Now that we understand why the symptom of insomnia is common in blind people we can treat it more effectively.

However, technologies that utilize quantum mechanics are becoming prevalent in our society so, scientific curiosity aside, it is important to increase our understanding of synchronization in a quantum context. This will help others design or identify things that utilize synchronization to further our understanding and level of technology.

Quantum synchronization has been observed in several systems, the most common of which is between optomechanical resonators[13, 14, 5]. They consist of an optical cavity with one of the mirrors connected to a spring. Light of intensity E is shone into this cavity which is detuned by a frequency $\Delta_j(t)$, where j denotes the jth oscillator. As the light transfers momentum to the cavity, the spring of coefficient k begins to oscillate. This can be coupled together through the transfer of phonons through the

surface that fixes the springs in place.

Systems like this have been shown to exhibit synchronization [13, 14], but are theoretically difficult to deal with. Most people consider only a pair of coupled oscillators and take the classical limit to create a "Kuramoto-like" pair of differential equations. For example, [13] uses a purely classical analysis and [14] looks at a classical Hamiltonian[3].

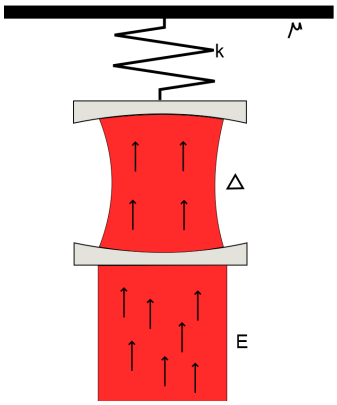

Figure 2.8: An optomechanical resonator

The current trend in the field of quantum synchronization is to create an analogy to Huygens pendulums and groups have done this with both optomechanical systems[13, 5] and light coupled atomic clocks[15]. Again, these systems have been shown to be capable of synchronizing, but are only between two oscillators.

Another thing to consider is that classical Kuramoto synchronization is an irreversible process. Once synchronization has been obtained, random fluctuations will never cause it to desynchronize. This is because equation (2.8) is not the full Hamiltonian description of the system. However, a lot of quantum mechanics is governed by Hamiltonian evolution which is necessarily time reversible. There are some quantum systems that are dissipative and therefore time irreversible do exist.

Reference [4] starts from the Hamiltonian of the Kuramoto model, which is the standard system of oscillators coupled to a thermal bath. They then introduce a term for the quantum noise and quantize the system. They have shown that this system can synchronize in some cases. However this is still a "top-down" approach, starting with the classical system and then working down to a microscopic description. Note also that this is a dissipative system; In this thesis we consider a purely Hamiltonian model.[4]

The question that I pose in this thesis is: can a Hamiltonian quantum analogy to the Kuramoto model synchronize at all? If it can synchronize, is it only transient or is it permanent? To the best of my knowledge there is no microscopic system that can map to the Kuramoto model.

The goal of this project is to work from the ground up to construct a microscopic model that will map to the Kuramoto model in the classical limit. I will then proceed to analyze the behaviour of said model. As most of the studies to date have been using a Kuramoto-like classical limit, my work will provide a platform for further work to

[3]This Hamiltonian includes an external light field, so synchronization of the oscillators is possible.

[4]This paper came out three days from the due date for this thesis, so I have not been able to incorporate it into my work.

continue with clear microscopic foundations.

Chapter 3

Quantum Theory

In the previous chapter we have covered the history of sync, building up to the Kuramoto model. Then we discussed why we are constructing a microscopic model. This leads us nicely into the quantum theory required for a quantum Kuramoto model.

3.1 Quantum Mechanics and Hamiltonian Evolution

A Hamiltonian quantum system can be represented by a state vector (or ket) $|\psi, t\rangle$, containing all of the information of the current state, and a Hamiltonian H, which describes the system's evolution and energy. The vectors lie in a Hilbert space, so there exists an inner product, and they are normalized such that $\langle\psi, t|\psi, t\rangle = 1$. Information contained by the state vector can be extracted by taking the expectation value of some hermitian operator, for example, the expectation value of some operator $\hat{A}$ is given by:

$$\begin{aligned}\langle A(t)\rangle &= \langle\psi, t|\hat{A}|\psi, t\rangle \\ &= \int_{-\infty}^{\infty}\int_{-\infty}^{\infty} dx\, dx' \langle\psi, t|x\rangle\langle x|\hat{A}|x'\rangle\langle x'|\psi, t\rangle\end{aligned} \tag{3.1}$$

In order to calculate these expectation values one generally projects the system a basis, as done in (3.1) where it was projected onto the continuous basis of position space. The time evolution of $|\psi, t\rangle$ is given by Schrodinger's equation:

$$i\hbar\frac{\partial}{\partial t}|\psi, t\rangle = \hat{H}|\psi, t\rangle \tag{3.2}$$

Another way to represent the state is by constructing a density operator defined by the outer product:

$$\hat{\rho} = |\psi, t\rangle\langle\psi, t| \tag{3.3}$$

which also contains all measurable information, as the expectation value of any operator $\hat{A}$ is

$$\langle A(t)\rangle = \langle\psi, t|\hat{A}|\psi, t\rangle = Tr\{A\rho(t)\} \tag{3.4}$$

and is thus equivalent to a state vector. This has a several important properties[1], but for our purposes we only need look at the equation of motion. In the Schrodinger

[1] For further details, see [16]

picture this is given by the Von Neumann Equation:

$$\dot{\rho}(t) = -\frac{i}{\hbar}[H, \rho(t)] \tag{3.5}$$

Note again that Hamiltonian evolution is time reversible. That is, setting $t \to -t$ will reproduce the same equations and dynamics. This is in contrast to dissipative systems as in reference [4], which can experience time irreversible behaviour.

Another important effect that quantum mechanics brings to a system is that there is a limitation on how accurately we can describe a system. This is encapsulated in the Heisenberg uncertainty principle, which for two operators $\hat{A}$ and $\hat{B}$, is given by:

$$\Delta A \, \Delta B \geq \frac{1}{2}|[\hat{A}, \hat{B}]| \tag{3.6}$$

with

$$\Delta A = \sqrt{\langle A^2 \rangle - \langle A \rangle^2} \tag{3.7}$$

The specific case of position and momentum is the one that people are more familiar with. This looks like:

$$\Delta x \, \Delta p \geq \frac{\hbar}{2} \tag{3.8}$$

where x and p are the position and momentum variables respectively.

What this boils down to is that for any operators that do not commute, there is a minimum uncertainty in a system. Where a classical system may be represented as a point in a phase diagram with p and x as the axes, a quantum system will be represented by a distribution with widths related in some way to its uncertainty. Furthermore this uncertainty can at times manifest as a form of noise[16].

3.2 The Wigner Function

A coherent state is the closest a quantum oscillator state can get to a classical oscillator and exhibits similar dynamics[16]. These states are defined as an eigenvector of the annihilation operator, $\hat{a}$, i.e.

$$\hat{a}|\beta\rangle = \beta|\beta\rangle \tag{3.9}$$

As we are looking to compare with the classical limit, it makes sense to look at coherent states in our quantum system. Because of this I will use the Wigner representation for my analysis. It is just one of many phase space representations of the density operators, but it is the most useful when dealing with coherent states and therefore the

one that is appropriate for us to consider.

For a classical probability distribution, the Fourier transform is called the characteristic equation[2] and is denoted as χ. The moments of the distribution are proportional to the derivatives of this function.

These ideas can be generalized to the quantum density operator. The symmetrically ordered characteristic function for a single bosonic mode is defined to be

$$\chi_W(\lambda, \lambda^*) = Tr\{\hat{\rho} e^{\lambda \hat{a}^\dagger - \lambda^* \hat{a}}\}, \tag{3.10}$$

where λ is a complex variable.

The symmetrically ordered moments of the annihilation and creation operators are given by

$$\left\langle \left\{ \hat{a}^s (\hat{a}^\dagger)^r \right\} \right\rangle = \left(\frac{\partial}{\partial \lambda} \right)^r \left(-\frac{\partial}{\partial \lambda^*} \right)^s \chi_W(\lambda, \lambda^*) \Big|_{\lambda=0} \tag{3.11}$$

where $\left\{ \hat{a}^s (\hat{a}^\dagger)^r \right\}$ refers to the symmetrically ordered product of the operators, e.g.

$$\left\{ \hat{a}^2 (\hat{a}^\dagger)^2 \right\} = \frac{1}{6} \left[(\hat{a}^\dagger)^2 \hat{a}^2 + \hat{a}^\dagger \hat{a} \hat{a}^\dagger \hat{a} + \hat{a}^\dagger \hat{a}^2 \hat{a}^\dagger + \hat{a} (\hat{a}^\dagger)^2 \hat{a} + \hat{a} \hat{a}^\dagger \hat{a} \hat{a}^\dagger + \hat{a}^2 (\hat{a}^\dagger)^2) \right]. \tag{3.12}$$

The Wigner function is defined as the Fourier transform of the symmetrically ordered quantum characteristic function and it exists for any density operator. That is,

$$W(\alpha, \alpha^*) = \frac{1}{\pi^2} \int d^2 \lambda e^{\lambda \hat{a}^\dagger - \lambda^* \hat{a}} \chi_W(\lambda, \lambda^*) \tag{3.13}$$

where α is the complex phase space variable and (3.11) becomes simply

$$\left\langle \left\{ \hat{a}^s (\hat{a}^\dagger)^r \right\} \right\rangle = \int d^2 \alpha \alpha^s (\alpha^*)^r W(\alpha, \alpha^*) = \overline{\alpha^s (\alpha^*)^r}. \tag{3.14}$$

As you can see, equation (3.14) behaves like a probability density and the bar in $\overline{f(\alpha, \alpha^*)}$ denotes the average of a function, f in phase space. However, $W(\alpha, \alpha^*)$ is called a quasi-probability density because it is not necessarily positive, but still contains all the information of a standard probability density.

Note that the phase space variables α and α^* are treated as independent variables, despite being complex conjugates of one another. Much like a traditional phase diagram represents a system with x and p, $\alpha = a + ib$ and it's complex conjugate contain equivalent information to x and p. Therefore, we can use phase space variables to represent our system and is the equivalent to projecting our system onto a new basis like

[2]Not to be confused with the interaction strength in chapter 5

in 3.1. The Wigner function can be viewed as the phase space distribution representing a quantum system in phase space, where a classical system would be a point.

Another thing to note about α is that is has the following relation to the occupation number of a state:

$$\overline{|\alpha|}^2 = n + \frac{1}{2} \tag{3.15}$$

where n is the number of bosons in the mode.

This can easily be generalized to n multiple modes with each α_j lying on orthogonal bases[3]. So,

$$W(\alpha, \alpha^*) \to W(\boldsymbol{\alpha}, \boldsymbol{\alpha^*}) = \prod_{j=1}^{N} W_j(\alpha_j, \alpha_j^*)$$

and

$$\overline{|\alpha_j|}^2 = n_j + \frac{1}{2} \tag{3.16}$$

Now in order to find how the Wigner function changes in time we need to find an equivalent of the Von Neumann equation (3.5). There is a direct mapping found by the following[16]:

$$\hat{a}_j\hat{\rho} \mapsto \left(\alpha_j + \frac{1}{2}\frac{\partial}{\partial\alpha_j^*}\right)W(\boldsymbol{\alpha}, \boldsymbol{\alpha^*}) \tag{3.17a}$$

$$\hat{a}_j^\dagger\hat{\rho} \mapsto \left(\alpha_j^* - \frac{1}{2}\frac{\partial}{\partial\alpha_j}\right)W(\boldsymbol{\alpha}, \boldsymbol{\alpha^*}) \tag{3.17b}$$

$$\hat{\rho}\hat{a}_j \mapsto \left(\alpha_j - \frac{1}{2}\frac{\partial}{\partial\alpha_j^*}\right)W(\boldsymbol{\alpha}, \boldsymbol{\alpha^*}) \tag{3.17c}$$

$$\hat{\rho}\hat{a}_j^\dagger \mapsto \left(\alpha_j^* + \frac{1}{2}\frac{\partial}{\partial\alpha_j}\right)W(\boldsymbol{\alpha}, \boldsymbol{\alpha^*}) \tag{3.17d}$$

There are then ways to deal with the resulting equations given in [16], provided the system is second order or lower. The noise from the quantum effects only comes into play through the second order terms and the initial conditions. If the system is only first order, then it is entirely deterministic and the only quantum effects are from the fact that there is uncertainty in the initial conditions.

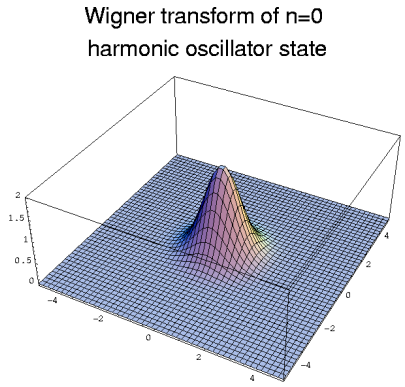

Figure 3.1: The Vacuum state. As stated above; coherent states are this same Gaussian distribution translated by β. Source of picture: [17]

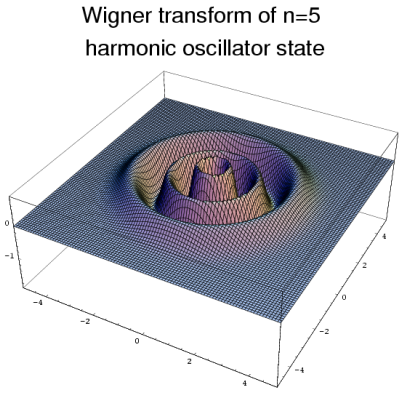

Figure 3.2: A number state. For large n, the outer ring becomes the dominant feature an can be approximated as a step function. Source of picture: [17]

3.2.1 Common Examples of Wigner states

There are several important examples of Wigner states:

- **Vacuum state** (Figure 3.1). This state is an oscillator with the lowest possible energy such as an empty optical cavity with only the zero point energy. This is a Gaussian distribution given by:

$$W(\alpha, \alpha^*) = \frac{2}{\pi} \exp\left(-2|\alpha|^2\right). \tag{3.18}$$

- **Coherent state**. This is what we have been looking at up until now. The state the closest resembles a classical harmonic oscillator behaviour and has the lowest uncertainty possible. This is the state that lasers emit and Bose-Einstein condensates are readily approximated to be in. This is given by

$$W(\alpha, \alpha^*) = \frac{2}{\pi} \exp\left(-2|\alpha - \beta|^2\right), \tag{3.19}$$

  where β is the coherent amplitude (given by (3.9)). As you can see this is just the Vacuum state translated by the coherent amplitude.

  For both this and the vacuum state the phase space variables are sampled with

[3]Here we have assumed that the state is separable and therefore, not entangled.

the initial conditions

$$\alpha = \beta + \frac{1}{2}(\eta_1 + i\eta_2) \tag{3.20}$$

where the η_j's are real, normally distributed variables.

- **Number or Fock state** (Figure 3.2). A state with an exact number of bosons. This is given by

$$W(\alpha, \alpha^*) = 2\frac{(-1)^N}{\pi} \exp\left(-2|\alpha|^2\right) L_N\left(4|\alpha|^2\right), \tag{3.21}$$

where L_N is the Laguerre polynomial of order N. However, for large N this can be approximated as a step function centered at $p = \frac{1}{2}(2N + 1 + 2\sqrt{N^2 + N})^{1/2}$, with

$$|\alpha_j| = p + \frac{\eta_j}{4p} \tag{3.22}$$

where η_j is a normal Gaussian random variable. These are then multiplied by a uniformly distributed random phase in the complex plane.

- **Squeezed state**. A coherent state with one of the quadratures "squeezed". By the uncertainty principle the other quadrature must expand. Can be viewed as a coherent state that has been squeezed, hence the name.

Chapter 4

Numerical Methods

As this project is primarily a numerical one it is important to make sure that the numerical methods we use are appropriate and will return accurate results. However, since we will be only solving coupled ordinary differential equations (ODEs), the straight-forward "ode45" function is all that we will require.

What I will be focusing on in this section is how to implement my numerical sampling and what compromises I have made in my simulations.

4.0.2 Sampling a Wigner Function

In the previous section we ended up with the time evolution of a quasi-probability density, the Wigner function (5.6). But how does one evolve this numerically? We do this through a process called sampling.

Say that we have a probability function with some rule governing how it behaves in time. If we wanted to numerically evolve this then one would take a set of points distributed by the probability function and see how the swarm of points behave.

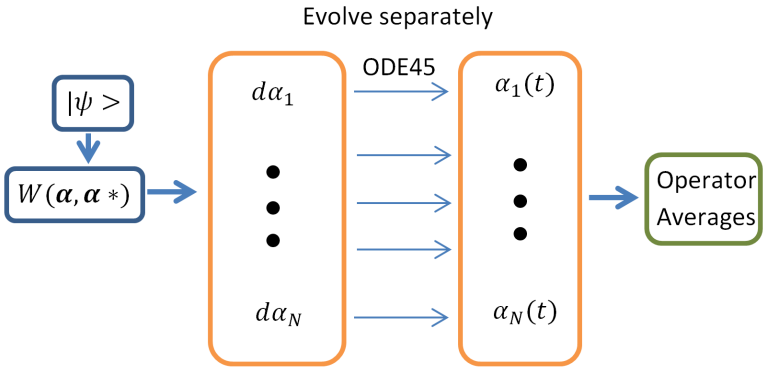

Figure 4.1: A flow chart of the process to numerically evolve interacting Wigner functions in time.

The Wigner function is a quasi-probability density, meaning that it can have negative values. However we are restricting our analysis to coherent states and large number states - which can be approximated to by (3.22)[1] - so this no longer something that we

[1]This is because the cumulative distribution is approximately a step function, so we can approximate the distribution itself like a delta function. That is the most simplistic treatment. We are using (3.22) which is better approximation and it has an uncertainty in amplitude.[18]

will worry about. Hence, we can evolve a non-interacting Wigner function in much the same way.

Our multi-mode Wigner functions work in exactly the same manner. The only difference is conceptual as instead of modeling a single mode with two variables as a two dimensional probability density, we are modeling a $2N$ dimensional probability density. This is evolved in the same way as above. We take a random selection of points and evolve each individually using our equation of motion.

This process is summed up in figure 4.1

4.0.3 Quality vs. Quantity

Up until now we have been making assumptions about the number of oscillators/modes that we are considering to be very large. You may have noticed a problem with the aims of this project in regards to this. We are wanting to simulate the phase space evolution of a quantum Kuramoto model, but the Kuramoto model is built on the basis that there is a large number of oscillators in the system. In fact, so many that we can approximate it as infinitely many. Simulating tens, even hundreds of thousands of oscillators is very time consuming, so it would be impractical to adhere strictly to these approximations.

To put some numbers to this I have produced two similar plots to 2.7. For both of these, the ODE solver was run separately for each step in K and averaged over 10 run-throughs. Figure 4.2was built with 10 oscillators and it took around 20 seconds to produce, whereas figure 4.3 has 100 oscillators and took about 10 minutes. Figure 2.7 took about 5 hours and that was with just 500 oscillators. It scales in time far faster than linearly with each new oscillator, so running this for 10,000 oscillators is completely impractical.

Compare the following two plots:

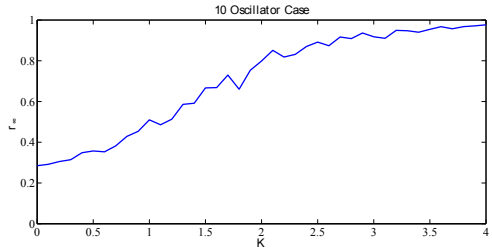

Figure 4.2: 2.7 reproduced with only ten modes and 40 data points.

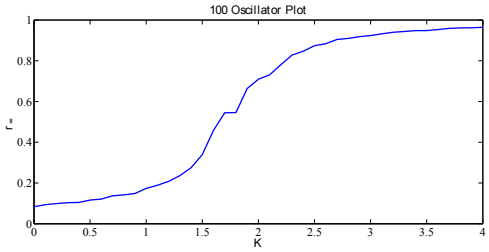

Figure 4.3: The same again with one hundred modes and 40 data points.

It is clear to see that there is significant difference between these two plots. Figure

4.2 contains very little of the shape in figure 2.7 and is very noisy, despite the averaging process. However, figure 4.3 is almost the same shape as figure 2.7. The biggest difference is that the curve at the critical value is gentler than the sharp transition that we should find.

One might think that there is a convergence in increasing the number of oscillators and they would be correct. In fact, the derivation of the critical coupling uses this fact[6, 2] and it has been shown that the Kuramoto model does indeed converge as $N \to \infty$ [6]. So we need to find a balance between accurate simulations and computation time.

In general I have been adapting the number of oscillators to each individual simulation. Before running a full simulation I would run a few quicker simulations to check what appropriate time steps and values for the number of modes/oscillators and occupation numbers. The appropriate values would be the values that led to computationally fast simulations, but did not detract from the qualitative behaviour of the system.

I would find these by starting at some values that produced what looked like accurate results and then run a short simulation for each parameter, taking a value higher and lower than the starting point. These would then be compared for how much the behaviour differed. If no qualitative difference could be seen the parameter would be moved toward more computationally favourable values and the process repeated. Conversely, if some difference could be seen in all three plots, then it would be moved towards computationally *un*favourable values. This would continue until the most computationally favourable, qualitatively sound values were found.

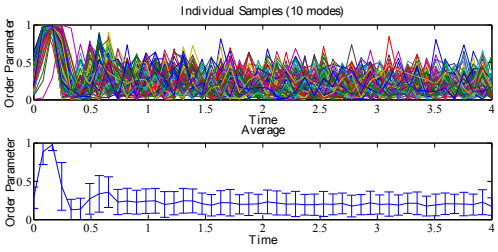

Figure 4.4: The time evolution of 100 samples for 10 modes.

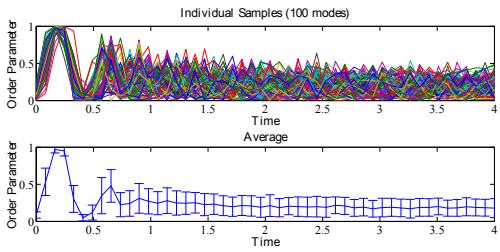

Figure 4.5: The time evolution of 100 samples for 100 modes.

An example that demonstrates this is drawn from the simulations in section A.2 (Figures 4.4 and 4.5). Here I have run the time evolution of the Wigner function for the same case, but with 10 and 100 modes. You can see from this that they both have the same qualitative behaviour: the peak, dip and smaller peak. There is, however, a difference in the size of the standard deviation towards the end. If using 50 modes

returned the same behaviour as figure 4.5, then I would be safe using 50 modes in my full simulation. This is because the qualitative behaviour behaviour has converged to a point where the difference between these cases is unnoticeable.[2]

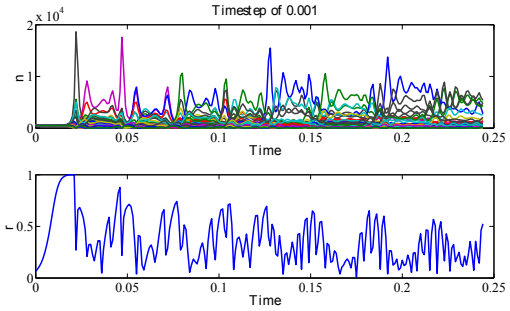

Figure 4.6: A plot of a large χ value with a time step of 0.001. There are 50 modes with $\bar{n} = 500$, $\chi = 0.005$ and $\Delta\omega = 1$.

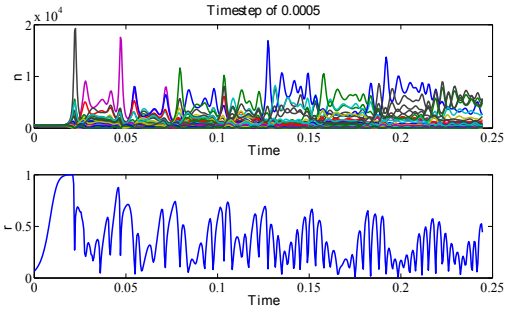

Figure 4.7: A plot of a large χ value with a time step of 0.0005. There are 50 modes with $\bar{n} = 500$, $\chi = 0.005$ and $\Delta\omega = 1$.

Figures 4.6 and 4.7 shows two plots of the average order parameter for very large coupling strength, one with twice as large time steps than the other. One can see straight away that both of these figures show the same behaviour. The plots have the same shapes and both of the simulations break down at the same point in time. Figure 4.7 has slightly sharper of the peaks and dips, but this can be chalked up to the higher resolution, as there is no difference in the overall behaviour.

This is the plot that had the most problems in the simulation. The strong coupling strength causes the system to fluctuate more than any other simulation and eventually break down. However, excluding the resolution, there is no qualitative difference between these two figures. This means that the tolerances and time steps we have used are sufficient to ensure numerical convergence.

[2]I would like to point out that increasing the number of particles in a system also changes the effective coupling strength. This is why there are differences in the sharpness in figure 4.5. One must account for this while searching for appropriate values for a simulation.

Chapter 5

Results

The goal of this thesis is to construct and analyze a quantum Hamiltonian that will collapse down to the classical Kuramoto model (2.4) when the appropriate limits are taken and explore its behaviour. Now that I have discussed the theory behind our system, we can move on to actually constructing the model itself.

5.1 Derivation

To do this we took a set of N harmonic oscillators; traps with a harmonic potential like that of a classical oscillator.

$$\hat{H}_{sp} = \sum_{j}^{N} \hbar\omega_j \hat{a}_j^\dagger \hat{a}_j \tag{5.1}$$

where ω_j is the frequency of the jth harmonic oscillator, or mode. The annihilation and creation operators, $\hat{a}_j$ and $\hat{a}_j^\dagger$, are the for bosons ans can be viewed as creating or destroying an individual boson in a mode. This describes the energy of a single, non-interacting particle, hence the subscript. We consider bosons for our trap due to the fact that they have a well defined classical limit[16].

Then we added an interaction potential that will yield the appropriate limits, as described in section 5.2.

$$\hat{H}_{int} = \sum_{\langle j,k \rangle}^{N} i\hbar\chi_{jk}(\hat{a}_j^\dagger \hat{a}_j \hat{a}_k^\dagger \hat{a}_j - \hat{a}_j^\dagger \hat{a}_k \hat{a}_j^\dagger \hat{a}_j) \tag{5.2}$$

where χ_{jk} is the interaction strength between the jth and kth modes and $\langle j,k \rangle$ denotes a double sum, excluding the cases where $j = k$.

The total Hamiltonian is the sum of these two:

$$\hat{H} = \hat{H}_{sp} + \hat{H}_{int} \tag{5.3}$$

In order to fully analyze the effects of quantum mechanics in this system it was my goal to see what effect quantum noise has on sync phenomena. For this I used some

phase space methods as follows. [1]

The Von Neumann equation of (5.3) for any density operator is:

$$\begin{aligned}\frac{\partial\hat{\rho}}{\partial t} &= -\frac{i}{\hbar}[\hat{H},\hat{\rho}] \\ &= -i\sum_j \omega_j(\hat{a}_j^\dagger\hat{a}_j\hat{\rho} - \hat{\rho}\hat{a}_j^\dagger\hat{a}_j) \\ &\quad ... + \sum_{<j,k>}\chi_{jk}(\hat{a}_j^\dagger\hat{a}_j\hat{a}_k^\dagger\hat{a}_j\hat{\rho} - \hat{\rho}\hat{a}_j^\dagger\hat{a}_j\hat{a}_k^\dagger\hat{a}_j - \hat{a}_j^\dagger\hat{a}_k\hat{a}_j^\dagger\hat{a}_j\hat{\rho} + \hat{\rho}\hat{a}_j^\dagger\hat{a}_k\hat{a}_j^\dagger\hat{a}_j)\end{aligned} \tag{5.4}$$

The mapping process is very long without much to be gained from following the process, and hence it is detailed in A.2. The end result only contains first and third order terms, the later can be neglected for the systems that we are working with as they vanish in the classical limit. Thus we find that

$$\begin{aligned}\frac{\partial W(\boldsymbol{\alpha},\boldsymbol{\alpha^*})}{\partial t} = -\sum_j \Bigg\{ \frac{\partial}{\partial\alpha_j}\Big[&- i\omega_j\alpha_j + \sum_{k\neq j}\chi_{jk}(\alpha_k^*\alpha_j\alpha_j \\ &... - 2\alpha_j^*\alpha_j\alpha_k + \alpha_k^*\alpha_k\alpha_k)\Big] + c.c.\Bigg\}W(\boldsymbol{\alpha},\boldsymbol{\alpha^*})\end{aligned} \tag{5.5}$$

or

$$\frac{\partial W(\boldsymbol{\alpha},\boldsymbol{\alpha^*})}{\partial t} = -\sum_j \left\{ \frac{\partial}{\partial\alpha_j}\left[-\frac{i}{\hbar}\frac{\partial H(\boldsymbol{\alpha},\boldsymbol{\alpha^*})}{\partial\alpha_j^*}\right] + c.c\right\}W(\boldsymbol{\alpha},\boldsymbol{\alpha^*}) \tag{5.6}$$

where $H(\boldsymbol{\alpha},\boldsymbol{\alpha^*})$ is our Hamiltonian(5.3) with $\hat{a}_j \mapsto \alpha_j$ and $\hat{a}_j^\dagger \mapsto \alpha_j^*$.

This yeilds the equations of motion for individual α_j:

$$\frac{d\alpha_j}{dt} = -\frac{i}{\hbar}\frac{\partial H(\boldsymbol{\alpha},\boldsymbol{\alpha^*})}{\partial\alpha_j^*}\,, \quad j = 1, ..., N \tag{5.7}$$

These equations are entirely deterministic as there were no second order terms in 5.6. This means that quantum noise does not effect how this system evolves, provided we are close to the classical limit. The only thing that we have to account for is the fact that the initial condition is a quantum state. This is done by taking the Wigner transform[2] of a density operator, ρ, to get the initial Wigner function appropriate to

[1] For more details on phase space representations and their applications see Quantum Noise [16] and reference [19]. Both of these contain some of the details given here and the later has details on how they can be applied to Bose-Einstein condensates, which exhibit similar behaviour to the quantum Kuramoto model.

[2] see A.2

the system. This has been done[18] for the states that we are interested in and the results are shown in section 3.2.1.

Note that up until now I have denoted the interaction strength as χ_{jk}, which allows for a non-equal coupling between different modes. I have kept it general on purpose as in a physical system the coupling strength will vary, but it will be symmetrical as the Hamiltonian must be a hermitian operator. However, the Kuramoto model is for a uniform coupling strength, so from now on I shall make the assumption that $\chi_{jk} = \chi$.

5.2 The Classical Limit

As I mentioned in section 3.1, the Hamiltonian is constructed such that in the appropriate limits it collapses to the Kuramoto mode, here I will show this. From (5.7), we have:

$$\dot{\alpha_j} = -i\omega_j\alpha_j + \chi\sum_{k\neq j}(\alpha_k^*\alpha_j\alpha_j - 2\alpha_j^*\alpha_j\alpha_k + \alpha_k^*\alpha_k\alpha_k) \tag{5.8}$$

Firstly we assume that every state is a coherent one with a large amplitude. With this we can approximate $\alpha_j \to \sqrt{n_j}e^{-i\theta_j}$, where n_j is the number occupation of the jth mode and θ_j it's phase. Substituting this in we get

$$\begin{aligned}\frac{e^{-i\theta_j}}{2\sqrt{n_j}}\dot{n}_j - i\sqrt{n_j}e^{-i\theta_j}\dot{\theta}_j = \\ - i\omega_j\sqrt{n_j}e^{-i\theta_j} + \chi\sum_{k\neq j}\left(n_j\sqrt{n_k}e^{-i(2\theta_j-\theta_k)} - 2n_j\sqrt{n_k}e^{-i\theta_k} + n_k^{3/2}e^{-i\theta_k}\right)\end{aligned} \tag{5.9}$$

equating real and imaginary parts gives

$$\dot{\theta}_j = \omega_j + \chi\sum_{k\neq j}^{N}\sqrt{n_jn_k}\Big(3 - \frac{n_k}{n_j}\Big)\sin(\theta_k - \theta_j) \tag{5.10a}$$

$$\dot{n}_j = -\chi\sum_{k\neq j}^{N}2\sqrt{n_jn_k}(n_k - n_j)\cos(\theta_k - \theta_j) \tag{5.10b}$$

Here you can see that the standard classical limit differs from the Kuramoto model in that it has $2N$ coupled differential equations for N oscillators. Each mode has two differential equations associated with it, one for phase and one for occupation number. However if we take one further limit, $n_j = \bar{n} = n_{tot}/N$, that is all of the occupation

numbers are equal, then we extract the Kuramoto model:

$$\dot{\theta}_j = \omega_j + \frac{2\chi n_{tot}}{N} \sum_{k \neq j}^{N} \sin(\theta_k - \theta_j) \tag{5.11a}$$

$$\dot{n}_j = 0 \tag{5.11b}$$

with an effective coupling constant

$$K_Q = 2\chi n_{tot} \tag{5.12}$$

So there exists a direct mapping to the Kuramoto model with an appropriate limit and numerical simulations of (5.10) in these limits do indeed behave exactly like the Kuramoto model (figure 5.1). This means that our Hamiltonian is what we were looking for; a quantum analogy to the classical Kuramoto model.

To make the comparison a bit more complete, we will cast this in terms of the mean field. First define an order parameter, as before by

$$re^{i\psi} = \sum_{k=1}^{N} \sqrt{\frac{n_k}{\bar{n}}} e^{i\theta_k} = \sqrt{\frac{N}{n_{tot}}} \sum_{k=1}^{N} \sqrt{n_k} e^{i\theta_k} \tag{5.13}$$

Multiplying both sides by $e^{-i\theta_j}$

$$re^{i(\psi - \theta_j)} = \sqrt{\frac{N}{n_{tot}}} \sum_{k=1}^{N} \sqrt{n_k} e^{i(\theta_k - \theta_j)} \tag{5.14}$$

Equating the real and imaginary parts yields

$$r \sin(\psi - \theta_j) = \sqrt{\frac{N}{n_{tot}}} \sum_{k=1}^{N} \sqrt{n_k} \sin(\theta_k - \theta_j), \tag{5.15a}$$

$$r \cos(\psi - \theta_j) = \sqrt{\frac{N}{n_{tot}}} \sum_{k=1}^{N} \sqrt{n_k} \cos(\theta_k - \theta_j). \tag{5.15b}$$

Then we substituting this into 5.10 we obtain:

$$\dot{\theta}_j = \omega_j + \frac{K_Q}{2}\sqrt{\frac{n_j}{Nn_{tot}}}r\sin(\psi-\theta_j)\sum_{k=1}^{N}\Big(3-\frac{n_k}{n_j}\Big), \tag{5.16a}$$

$$\dot{n}_j = -K_Q\sqrt{\frac{n_j}{Nn_{tot}}}r\cos(\psi-\theta_j)\sum_{k=1}^{N}(n_k-n_j). \tag{5.16b}$$

as $n_{tot} \gg n_j$, this simplifies to:

$$\dot{\theta}_j = \omega_j + \frac{K_Q}{2}\sqrt{\frac{n_j}{Nn_{tot}}}\big(3N-\frac{n_{tot}}{n_j}\big)r\sin(\psi-\theta_j), \tag{5.17a}$$

$$\dot{n}_j = -K_Q\sqrt{\frac{n_j}{Nn_{tot}}}\big(n_{tot}-2Nn_j\big)r\cos(\psi-\theta_j). \tag{5.17b}$$

Here you can see that it this system can be modeled in a similar way to the Kuramoto model. Each oscillator is coupled together only by (5.13) and can effectively be modeled as pairs of independent coupled equations that are only affected by the mean field. However the effective coupling strength is proportional to the number in the mode itself, as well as how ordered the system is.

5.2.1 Simulations of Classical Limit

These simulations contain the key findings from the numerical analysis of (5.10). This first series of simulations are for 100 modes.

The first thing to look at is whether the simulations agree with the analytical theory in the Kuramoto limit. So setting all of the occupation numbers to be equal produces figure 5.1. This was for a coupling strength greater than critical, so we have the same behaviour as the Kuramoto model itself.

To see whether this is a stable equilibrium or not we now distribute the occupation numbers normally and take the width, Δn, to be far less than the magnitude[3]. If unstable, it should diverge from this stationary point. This is indeed what we find, as you will see in subsequent figures.

Figures 5.2 and 5.3 are two cases of the common behaviour for $K_Q i > K_c$. Here you can see that the initial distribution in number stays very small for a time before one or more modes blows up. This eventually settles into chaotic behaviour. However, looking at the order parameter we can see that for the time where the number distribution is

[3]Now that n_{tot} as an element of randomness in its definition, the value of K_Q will also have a degree of randomness. But for all simulations where $\Delta n = 1$, this randomness will be much less than 1 part in 1000, so I will ignore it.

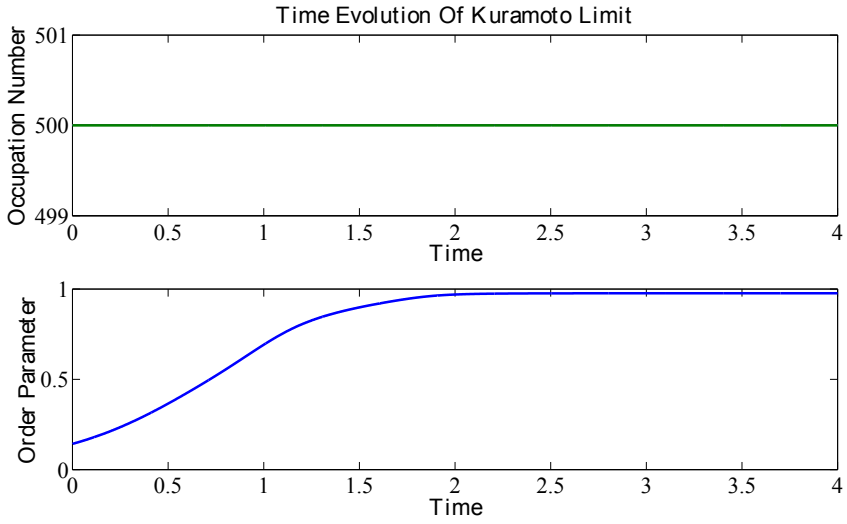

Figure 5.1: The Kuramoto limit. Here the system spontaneously synchronizes as in figure 2.5 and the occupation number does not change. $K_Q = 2.5$, $\Delta\omega = 1$ and $\Delta n = 0$.

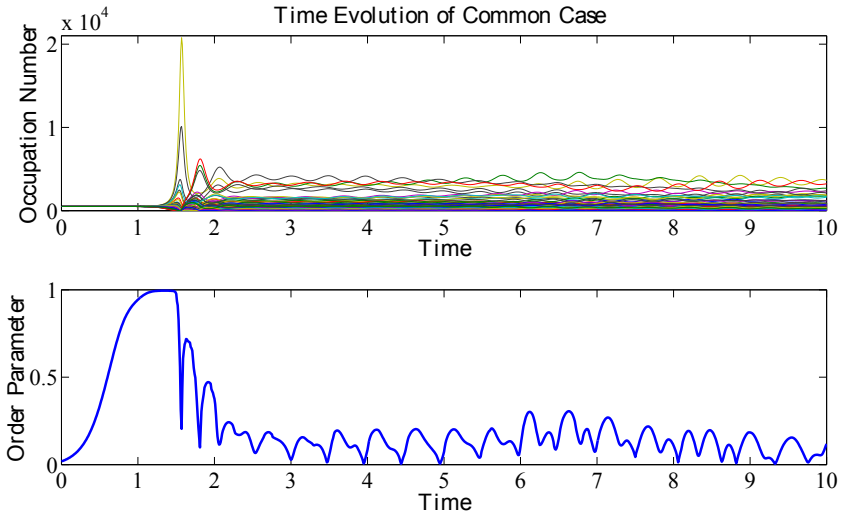

Figure 5.2: 100 modes, $K_Q = 5$, $\Delta\omega = 1$ and $\Delta n = 0.1$.

approximately flat, the system behaves like the classical Kuramoto model and even synchronizes for a time. Thus we see transient synchronization. This agrees with the analytics in that the synchronization is only transient and unstable as is quickly degrades after a time T_s to a highly chaotic state.

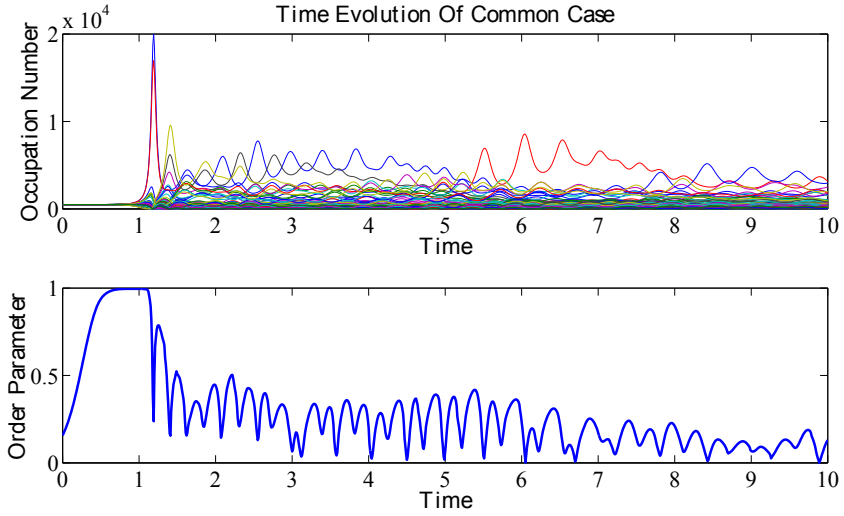

Figure 5.3: 100 modes, $K_Q = 5$, $\Delta\omega = 1$ and $\Delta n = 0.1$.

You might be wondering, what with the huge fluctuations in number, if the total number of bosons is conserved. In figure 5.4 we show the typical evolution of n_{tot}, from which it is clear that the total population is conserved to at most one part in 10^4. We ensure that this is the case for all our simulations.

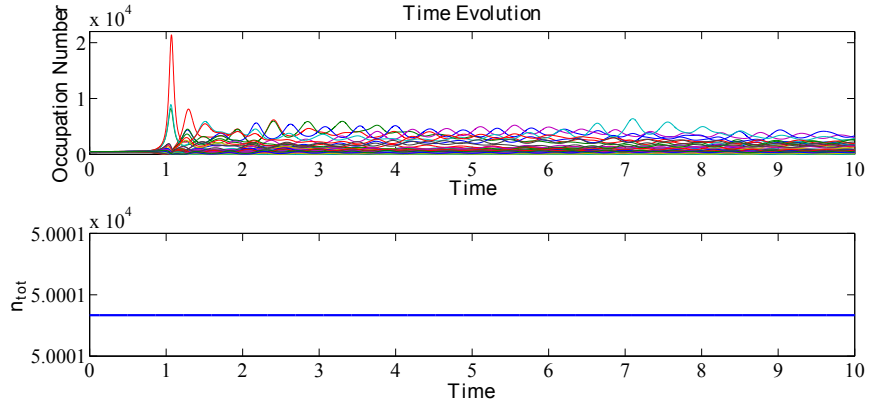

Figure 5.4: 100 modes, $K_Q = 5$, $\Delta\omega = 1$ and $\Delta n = 1$. The second plot shows that the variation in total number of bosons is so insignificant that it cannot be seen here.

There was, however, a significant problem that came from running the simulations of equations (5.10). When deriving these we had to divide by the number in a state n_j. However if this number goes to zero, then the simulation would break down, severely

limiting the length of time it can run for. When this would happen was largely based on chance, but since the number interaction strength increases with K_Q, it would occur more often for higher values of K_Q.

This problem does not occur in the Wigner formulation as there is no need to divide by any variable that can vanish in the derivation.

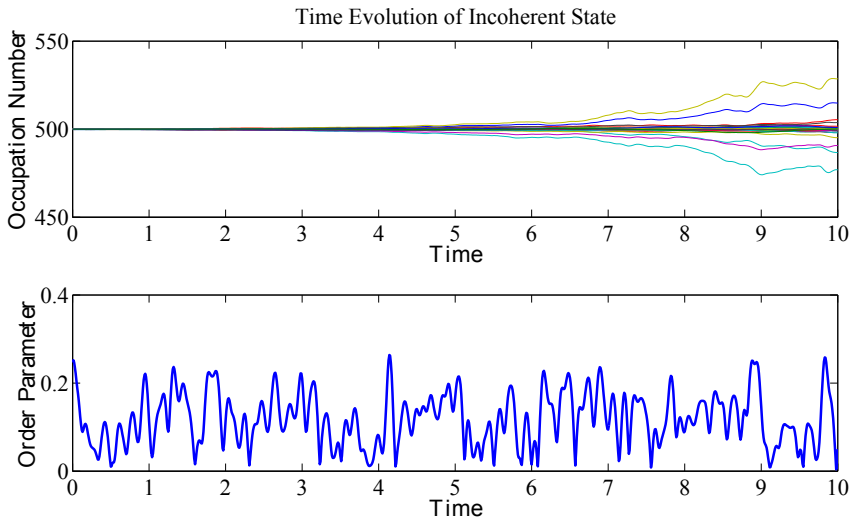

Figure 5.5: 100 modes, $K_Q = 5$, $\Delta\omega = 20$ and $\Delta n = 1$

In the classical Kuramoto model there was a transition between incoherent and coherent when either increasing χ or lowering $\Delta\omega$. In Figure 5.5 we show the results for $\Delta\omega$ chosen to be so large that the system cannot synchronize. Looking at the order parameter, we see that it is behaving incoherently. Interestingly, the mode occupation shows more stability in the incoherent system than the transient synchronized system.

Increasing $\Delta\omega$ had no effect on the length of the transient synchronization, T_s, defined previously. It only lowered the maximum level of synchronization it will obtain.

In varying the interaction strength, χ, I found this to have an inverse effect on T_s. But since it also increases the speed of which the system synchronizes the same level is reached.

As I have stated before, increasing χ causes numerical problems. However increasing it beyond a certain value causes the system itself to develop a strange, pseudo-periodic behaviour where the order parameter exhibits a revival after the initial synchronization. We also see large peaks in occupation number for certain modes appear sporadically throughout all times beyond T_s. Figures 5.6 and 5.7 are examples of this and it could be an indication that the weak coupling assumption is reaching it's limit.

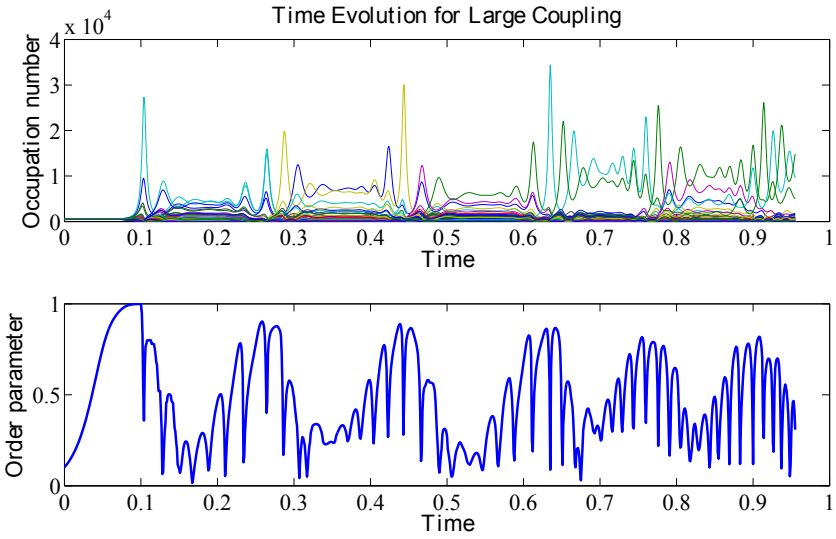

Figure 5.6: 100 modes, $K_Q = 50$, $\Delta\omega = 1$ and $\Delta n = 1$

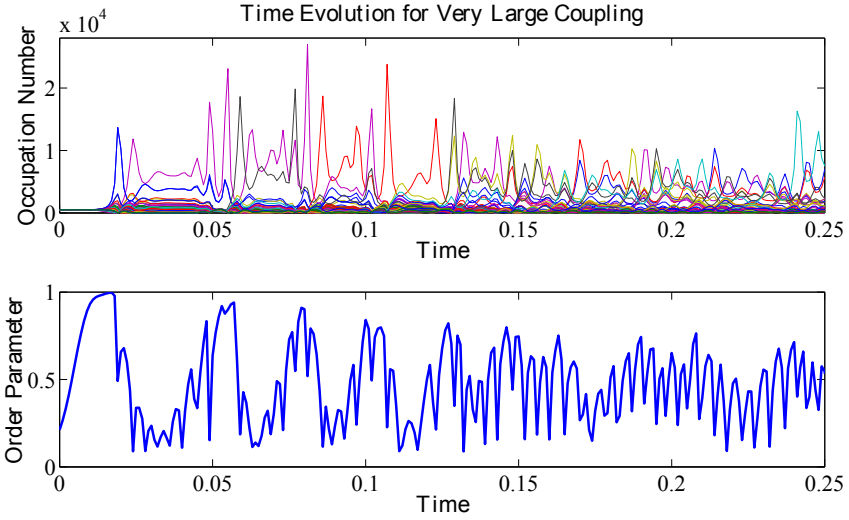

Figure 5.7: 100 modes, $K_Q = 250$, $\Delta\omega = 1$ and $\Delta n = 1$

Note that they don't run for the same time intervals. This is because the simulations crashed due to the afore-mentioned problem.

Finally, I looked into increasing the width of the number distribution, Δn (Figures

5.8 and 5.9). With this I found what I expected: the only effect that this had was shortening the time T_s with no effect on the speed of synchronization. This meant that the level of synchronization was lowered accordingly.

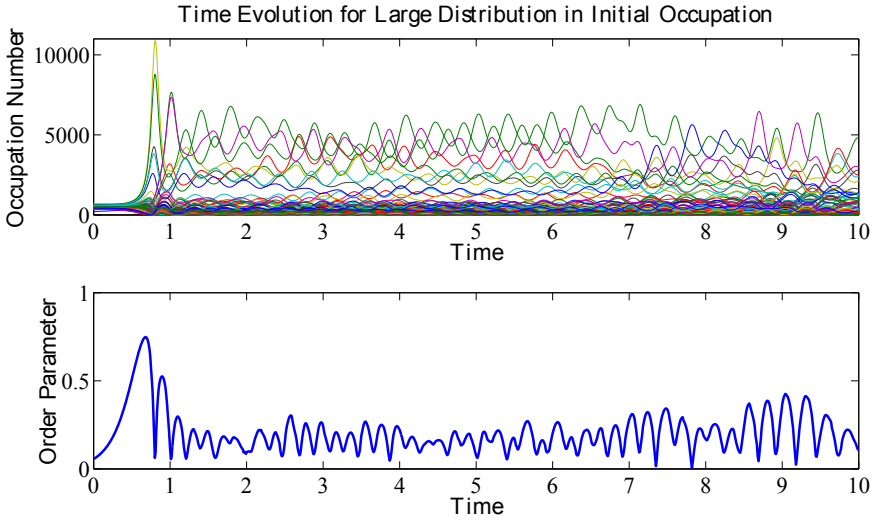

Figure 5.8: 100 modes, $K_Q \approx 5$, $\Delta\omega = 1$ and $\Delta n = 80$

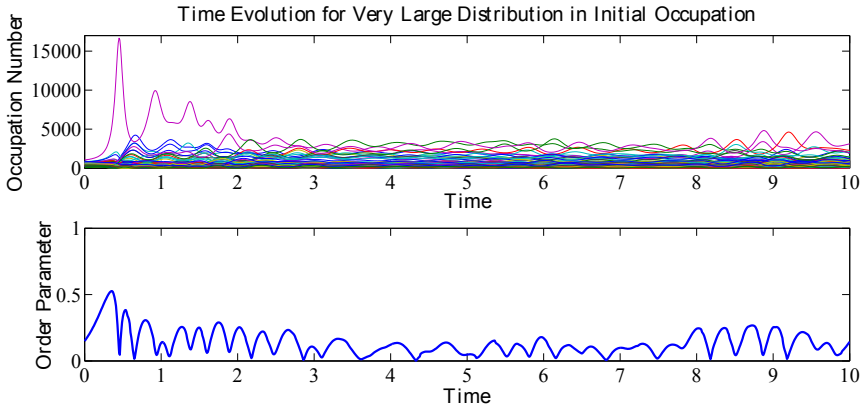

Figure 5.9: 100 modes, $K_Q \approx 5$, $\Delta\omega = 1$ and $\Delta n = 200$

5.2.2 Linear stability analysis

It is plain to see from (5.17) that taking $r = 0$ is a stationary point to any number of modes. However, since $r = 1$ implies that all $\theta_j = \psi$ it is also a stationary point for a

flat number distribution, i.e. $n_j = \bar{n}$ for all j. The question is what are the properties of these stationary points and are any of them stable. To find out I performed a linear stability analysis.

Let

$$\boldsymbol{x} = \begin{pmatrix} \boldsymbol{\theta} \\ \boldsymbol{n} \end{pmatrix}, \dot{\boldsymbol{x}} = \boldsymbol{f}(\boldsymbol{x}) = \begin{pmatrix} \boldsymbol{f}_\theta \\ \boldsymbol{f}_n \end{pmatrix}$$

where $\boldsymbol{f}(\boldsymbol{x})$ is the RHS in the equations (5.15).

The incoherent state is actually an infinite set of states due to the arbitrary combinations of phases, so this will be too complicated to analyze here. So I will instead look at the Kuramoto synchronized limit where $n_j = \bar{n}$. This is also an infinite series of points, however it has a clear relation between the phases, so we can gain some knowledge of it.

Around a point, $\boldsymbol{x_0}$, we can model the derivative as a first order expansion in $(\boldsymbol{x} - \boldsymbol{x_0})$.

$$\dot{\boldsymbol{x}} = \boldsymbol{f}(\boldsymbol{x_0} + \Delta\boldsymbol{x}) \simeq \nabla \boldsymbol{f}(\boldsymbol{x_0}) \cdot \Delta\boldsymbol{x} \tag{5.18}$$

for some small displacement $\Delta\boldsymbol{x}$. About an arbitrary point this yields:

$$\begin{aligned}
\frac{\partial f_{\theta_j}}{\partial \theta_j} &= -\chi \sum_{k \neq j} \sqrt{n_j n_k}\Big(3 - \frac{n_k}{n_j}\Big) \cos(\theta_k - \theta_j), \\
&\qquad\qquad \frac{\partial f_{\theta_j}}{\partial \theta_k} = 2\chi \sqrt{n_j n_k}\Big(3 - \frac{n_k}{n_j}\Big) \cos(\theta_k - \theta_j) \\
\frac{\partial f_{\theta_j}}{\partial n_j} &= -2\chi \sum_{k \neq j} \Big(\frac{3}{2}\sqrt{\frac{n_k}{n_j}} + \frac{1}{2}\Big(\frac{n_k}{n_j}\Big)^{3/2}\Big) \sin(\theta_k - \theta_j), \\
&\qquad\qquad \frac{\partial f_{\theta_j}}{\partial n_k} = 2\chi \big(\frac{3}{2}\sqrt{\frac{n_j}{n_k}} - \frac{3}{2}\sqrt{\frac{n_k}{n_j}}\Big) \sin(\theta_k - \theta_j) \\
\frac{\partial f_{n_j}}{\partial \theta_j} &= -2\chi \sum_{k \neq j} \sqrt{n_j n_k}\big(n_k - n_j\big) \sin(\theta_k - \theta_j), \\
&\qquad\qquad \frac{\partial f_{n_j}}{\partial \theta_k} = 2\chi \sqrt{n_j n_k}\big(n_k - n_j\big) \sin(\theta_k - \theta_j) \\
\frac{\partial f_{n_j}}{\partial n_j} &= 2\chi \sum_{k \neq j} \sqrt{n_k}\Big(\frac{n_k}{2\sqrt{n_j}} - \frac{3}{2}\sqrt{n_j}\Big) \cos(\theta_k - \theta_j), \\
&\qquad\qquad \frac{\partial f_{n_j}}{\partial n_k} = -2\chi \sqrt{n_j}\Big(\frac{3}{2}\sqrt{n_k} - \frac{n_j}{2\sqrt{n_k}}\Big) \cos(\theta_k - \theta_j)
\end{aligned} \tag{5.19}$$

For $n_j = \bar{n}$ this becomes:

$$\begin{aligned}
\frac{\partial f_{\theta_j}}{\partial \theta_j} &= -2\chi\bar{n}\sum_{i\neq k}\cos(\theta_k-\theta_j) \quad , \quad \frac{\partial f_{\theta_j}}{\partial \theta_k} = 2\chi\bar{n}\cos(\theta_k-\theta_j) \\
\frac{\partial f_{\theta_j}}{\partial n_j} &= -2\chi\sum_{k\neq j}\sin(\theta_k-\theta_j) \quad , \quad \frac{\partial f_{\theta_j}}{\partial n_k} = 0 \\
\frac{\partial f_{n_j}}{\partial \theta_j} &= \frac{\partial f_{n_j}}{\partial \theta_k} = 0 \\
\frac{\partial f_{n_j}}{\partial n_j} &= 2\chi\bar{n}\sum_{k\neq j}\cos(\theta_k-\theta_j) \quad , \quad \frac{\partial f_{n_j}}{\partial n_k} = -2\chi\bar{n}\cos(\theta_k-\theta_j)
\end{aligned} \tag{5.20}$$

This is too complex to see the dynamics, but when we look only at the $\theta_j = \psi$ case this collapses down to:

$$\nabla \boldsymbol{f}(\boldsymbol{x_0}) = \begin{pmatrix} -2\chi n_{tot} & 2\chi\bar{n} & ... & 0 & 0 \\ 2\chi\bar{n} & -2\chi n_{tot} & ... & 0 & 0 \\ ... & ... & ... & ... & ... \\ 0 & 0 & ... & 2\chi n_{tot} & -2\chi\bar{n} \\ 0 & 0 & ... & -2\chi\bar{n} & 2\chi n_{tot} \end{pmatrix}$$

which can be seen to be stable in phase, but unstable in number. From this we can conclude that if the system is in the Kuramoto stationary point, a small fluctuation will cause the occupation number to destabilize. Therefore permanent synchronization is not possible.

5.2.3 Two Mode Case

To gain a qualitative feel for the behaviour found in 5.2.1 and 5.2.2 I looked at the two mode case. As the coupling between all of the modes is of the same form, restricting to the two mode case will make the dynamics easier to grasp while containing the essence of the large N behaviour. Generalizing to larger N only amounts to adding similar off diagonal terms.

This switch allows us to analyze another case's linear behaviour. As the previous sections concluded, the Kuramoto synchronized state is unstable in occupation number. So what happens in the other extreme? Let's take a look at the behaviour if a single mode has the vast majority of bosons and the other has only a few. In terms of simplifying (5.19) for the two mode case this manifests as $n_1 \gg n_2$ and we will take $n_2 \approx 1$ so as to avoid dividing by zero, therefore $n_1 \approx n_{tot}$. Simulations show that when behaviour like this happens the order parameter is small (figure 5.10), so we will include that $(\theta_1)_0 - (\theta_2)_0 = \pi$ as this makes $r = 0$ at $\boldsymbol{x_0}$. Now we have:

$$\Delta \boldsymbol{x} = \begin{pmatrix} \Delta n_1 \\ \Delta n_2 \\ \Delta \theta_1 \\ \Delta \theta_2 \end{pmatrix}$$

and

$$\nabla \boldsymbol{f}(\boldsymbol{x_0}) = \begin{pmatrix} 3\chi\sqrt{n_{tot}} & -3\chi\sqrt{n_{tot}} & 0 & 0 \\ \chi n_{tot}^{\frac{3}{2}} & -\chi n_{tot}^{\frac{3}{2}} & 0 & 0 \\ 0 & 0 & -3\chi\sqrt{n_{tot}} & -\chi n_{tot}^{\frac{3}{2}} \\ 0 & 0 & 3\chi\sqrt{n_{tot}} & \chi n_{tot}^{\frac{3}{2}} \end{pmatrix}$$

which is unstable in n_1. It's not clear straight away, but a slight change in n_1 will change $\dot{n}_1$ proportional to the square root of n_{tot}. Conversely, a small change in n_2 will change it proportional to $n_{tot}^{\frac{3}{2}}$ and will therefore dominate. So I would expect the occupation numbers to flatten out.

Comparing these two cases that I have looked at one would expect the 2 mode case to oscillate in number and this is what we find. Figure 5.10 is the case where the frequencies are very close to one another. Here we can see that the two modes do indeed oscillate in number as predicted. However they also have an almost periodic behavior in order parameter too.

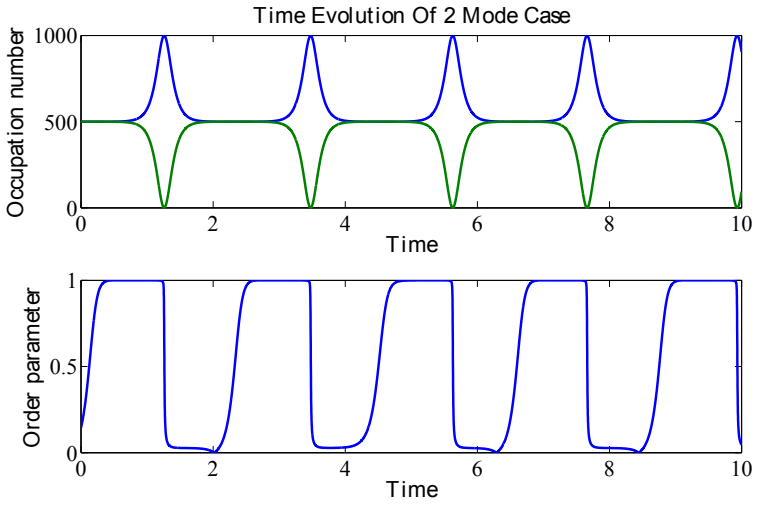

Figure 5.10: 2 modes, $K_Q = 5$, $\Delta\omega = 1$ and $\Delta n = 1$

Now, if they were two non-interacting oscillators, then the order parameter would have the character of a sine function. Here we can see that there is a sharp dip in

r when the occupation numbers are at opposite extremes. The order parameter then stays around zero until the number states have flattened out again. Then, like previous simulations, the system stays in perfect sync until the number states have blown up again. Based on the stability analysis, and the fact that the order parameter has the same period as the number oscillations leads me to conclude that this is very different from the normal sinusoidal behaviour in the non interacting case.

It should be noted that, while figure 5.10 shows that the pattern repeats, it does not have a constant period. If you look closely at it you should be able to see that some of the peaks are further apart than others. However the average frequency is consistent for a given K_Q and has a direct proportionality to it. Another curiosity is that the mode with the largest occupation number will always return to the initial values and the one with the majority will never change.

Increasing the distribution in occupation number does not change the dynamics, only how close the number oscillations are to one another. For example, if the two states start with a difference in number of 100 then there will still be the same oscillations seen in figure 5.10. The only difference is that instead of both modes returning to $n = 500$, they would return to their initial conditions of a 100 particle difference.

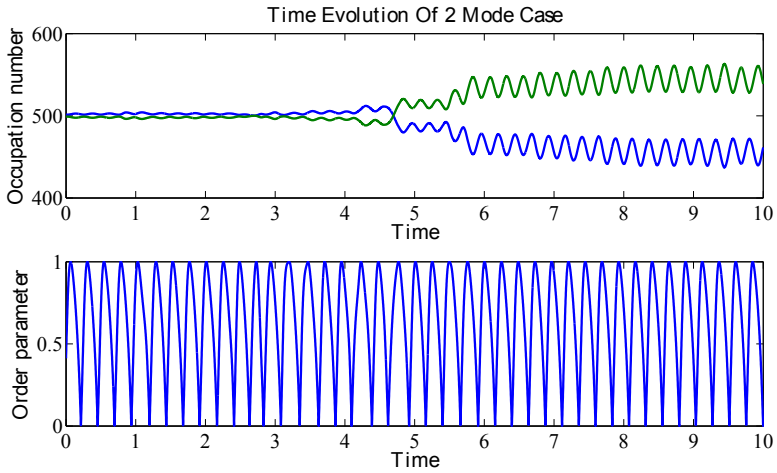

Figure 5.11: 2 modes, $K_Q = 5$, $\Delta\omega = 10$ and $\Delta n = 1$

Figure 5.11 is what 2 modes look like when their frequencies are too far apart to classically synchronize[4] at all. The number dynamics consist of a series of oscillations between the two modes of a relatively constant size. The size and separation of these oscillations are unpredictable and seemingly random. While the oscillations are of

[4]By equation (5.12)

a relatively consistent period, there is no longer the relation between K_Q and the frequency as opposed to in figure 5.10. The mode with the most bosons does change in this case.

5.3 Phase Space Simulations

Now we will look at numerically simulating equation (5.8) using the method described in section 4.0.2.

5.3.1 Simulation

The states [5] that we will look at are the coherent and Fock or number states, both with a large amplitude[6]. The large amplitude Fock states are represented by a spike in $|\alpha|$ which is rotationally symmetric. The coherent states are represented by Gaussian distributions displaced by β.

The simplest case for coherent states is taking all of the modes to have the same β. This is a quantum analogy to synchronized classical oscillators. However, I am wanting to look at the emergence of synchronization, so I will take $\beta_j = |\beta| \exp(i\theta_j)$, where θ_j are uniformly distributed on $[0, 2\pi)$ for the jth mode. This is the closest analogy to the classical incoherence.

Since we are looking at a large number of modes, N, this will yield a rotationally symmetric distribution at $|\beta|$ of a Gaussian profile in amplitude. As the amplitude is proportional to occupation number, this total distribution will look very similar to a Fock state. Because of this, using Fock states is a way that we can simulate the dynamics of large N coherent states for less modes. Fock states produce clearer results for the phase dynamics due to the fact that the initial distributions were sharper and more consistently distributed than the coherent states' for computationally viable number of modes. For these reasons I will only cover Fock states in this section, but I have looked at and gained similar results for coherent states too.

Note that for large amplitudes, increasing the occupation number only changes the dynamics by increasing the interaction strength and is therefore not important to focus on.

The first important thing to note is that the ideal Kuramoto synchronized state, like in figure 5.1, is unattainable with this numerical method. The computational error (of order 10^{-16}) in representing the magnitude of each α_j is enough to make the system

[5] see section 3.2.1

[6] For all of my simulations I have been using 50^2 bosons per mode.

diverge from this state when evolving in time. This is to be expected and is nothing to be worried about since this is an unstable stationary point.

Soon I will be showing a couple of three dimensional plots, but before that it will probably be helpful to see the dynamics of an individual run. A large number of the following figures will be divided into two separate plots. The first plot is of the order parameters from individual samples and the second is the average with one standard deviation shown for each data point.

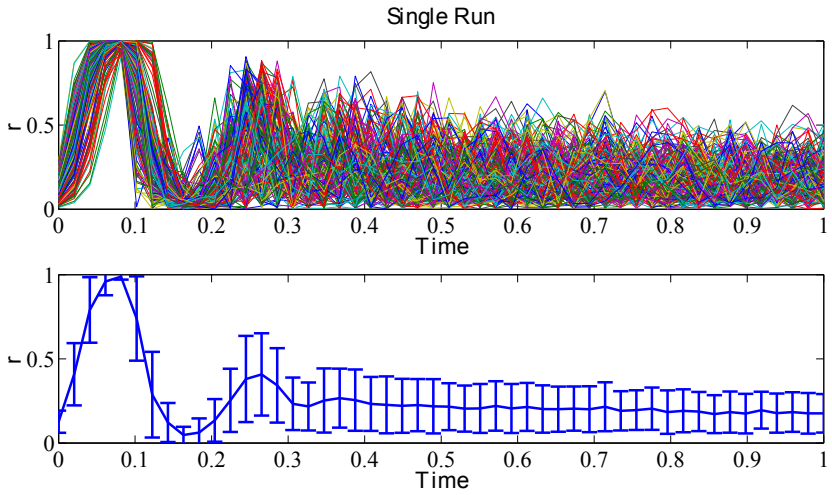

Figure 5.12: 50 modes, 300 samples with $K_Q = 125$ and $\Delta\omega = 1$

The majority of the transient synchronization observed had a similar shape to figure 5.12. There is the initial jump from incoherent to synchronized. This is followed by a drop back to an incoherent state with a very low standard distribution. Then the system oscillates in order parameter a few times until it has reached a noisy, dynamic equilibrium. This peak and dip occurs for most cases where transient synchronization is found, with some exceptions that I will be getting to.

A quick aside: as you can see in figure 5.13 the difference in the number of bosons from the previous simulation is less than 0.35 for the depicted sample from an initial total of 50,100 bosons. For all samples in figure 5.12, the maximum difference was about 0.51. As the center of the distribution in number sits on 50,000 bosons a back-of-the-envelope calculation shows that the error is of order 10^{-5}. This is well within a tolerable level of error in total number. As the coupling strength increases, this error did increase, but only to a maximum of about 1. This is still small enough compared to the total number of bosons that they can effectively be said to be conserved.

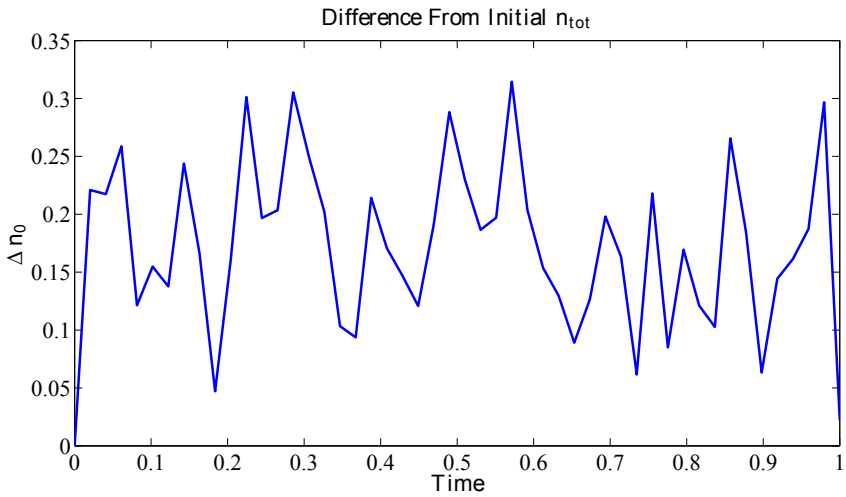

Figure 5.13: The change in n_{tot} for a single sample in figure 5.12. The initial number of bosons for this run was almost 50,100.

The distribution of natural frequencies

In figure 5.14 I have scanned across the width of the natural frequency distribution, $\Delta\omega$, for a reasonable coupling strength of $K_Q = 9$. This figure encapsulates all of the behaviour dependent on the initial frequency distribution. I will break this plot down and show individual slices to make it easier to understand, but we can clearly see some of the behaviour that I have mentioned earlier here. For the smaller frequency distributions we can see the early period of transient synchronization followed by a drop to $r \approx 0$. We can even clearly see three diminishing oscillations in r that follow this which here are the three cyan bands. The values of r after these bands take almost the full four dimensionless units of time to reach their incoherent stable state. All of these values are similar to figure 5.12 in behaviour.

I would like to draw your attention to a few features of this pot. The first is that for all cases where transient synchronization is possible, the period of synchronization, T_s, is independent of the value of $\Delta\omega$.That is, the width of the red band does not change for values lower than around 1 in the y axis. However, for increasing values the following dip shrinks in width and eventually vanishes. The cyan bands move closer to T_s to fill this space, until they eventually vanish too.

The values where there is no further peaks after the initial synchronization are interesting in that they very quickly reach their stable end state, when the smaller values of $\Delta\omega$ take much longer to stabilize. This takes the form of the horizontal trough at around $\log_{10}(\Delta\omega) \approx 1.3$. This is demonstrated in figure 5.15 and you can also see, by comparing it with figure 5.16, that the standard deviation is also a lot

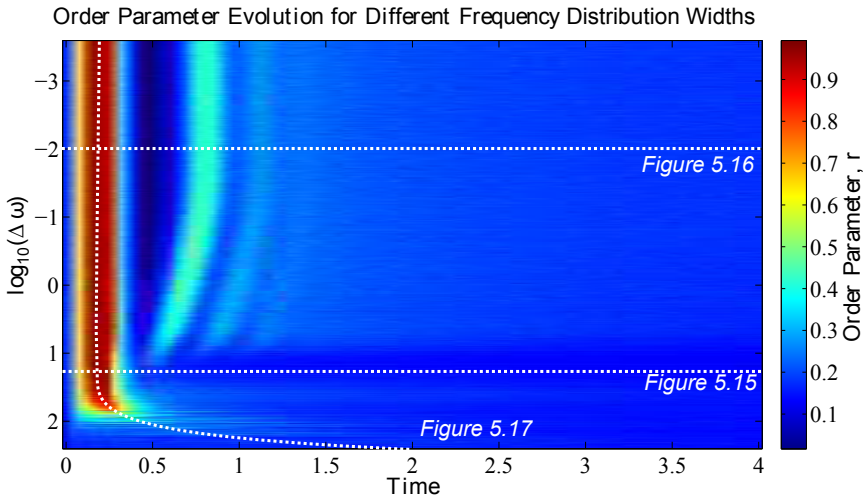

Figure 5.14: 50 modes, 500 samples with $K_Q = 45$ and 900 bosons per mode.

smaller for this case, even when the figure 5.16 has reached it's stable point.

This is a surprising discovery as it means that there exists a sweet spot where the distribution yields a lower uncertainty in it's incoherent state than all other points for a given K_q. It is surprising because one would expect the system to have a smaller deviation for more similar oscillators, as opposed to what we find. I cannot think of a explanation for why this might be, and yet all of my simulations on the matter yield that same result.

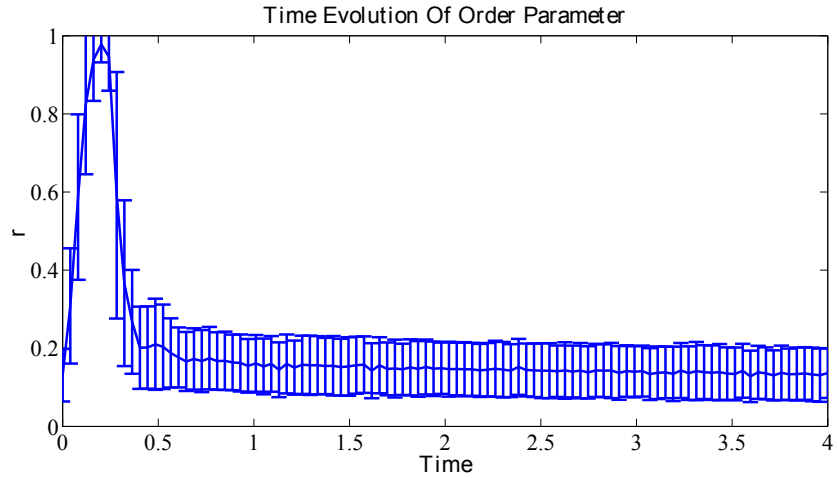

Figure 5.15: 50 modes, 500 samples with $K_Q = 45$ and $\Delta\omega = 16.98$ and 900 bosons per mode.

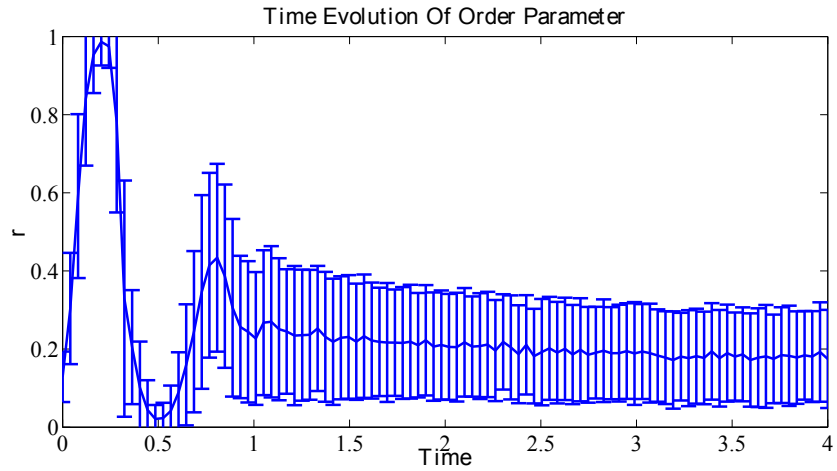

Figure 5.16: 50 modes, 500 samples with $K_Q = 45$ and $\Delta\omega = 0.01$ and 900 bosons per mode.

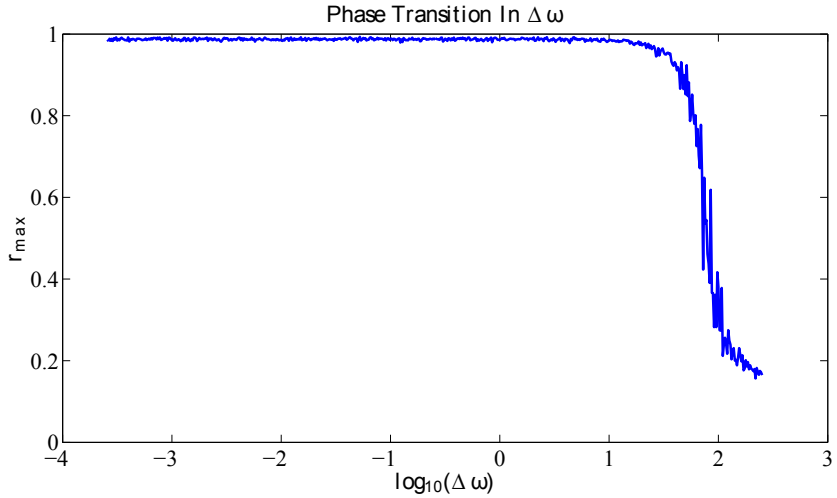

Figure 5.17: 50 modes, 500 samples with $K_Q = 45$ and 900 bosons per mode.

Figure 5.17 is a plot generated by taking the maximum of the order parameter for each value of $\Delta\omega$ in figure 5.14. You can see in the earlier figure that there is a value of $\Delta\omega$ for which the transient sync is no longer possible. In this figure we find that the value for which $r_{max} = 0.5$ is in the range $1.85 \leq \log_{10}(\Delta\omega) \leq 1.94$ or $70.7 \leq \Delta\omega \leq 87.1$, which matches the classical critical coupling value of $K_c = 125$.

Due to the way that this plot was constructed the lower values of r_{max} are prone to noise. This is unavoidable due to the fact that the synchronization is transient; in the classical model one can average the values of all points beyond synchronization,

whereas here we can't do that and have to deal with the noise. However this does not get in the way of the dynamics of the system, it only adds to the uncertainty of the numbers that we can extract from this system.

This phase transition further cements this model as a quantum analogy to the Kuramoto model as this is a transient version of the transition discussed in section 2.1 and matches with the results from section 5.2.1.

The coupling strength, K_Q

Here I will be looking at how changing the coupling strength changes the dynamics and highlight the interesting features, like I did in the previous section for $\Delta\omega$. However it is important for me to point out a few details associated with varying the coupling strength.

It is important to note that while we do not have the problem of dividing by zero as we did in the classical limit, the computational time increases with K_Q. Increasing K_Q will shorten the timescales of T_s and the subsequent features of a plot. Both of these relations make scanning over large ranges of K_Q impractical, as for time-steps that are computationally reasonable the non-equilibrium behaviour for the higher values could be skipped over and only a part of them simulated for the lower values. For this reason I have cut the scanning into smaller chunks.

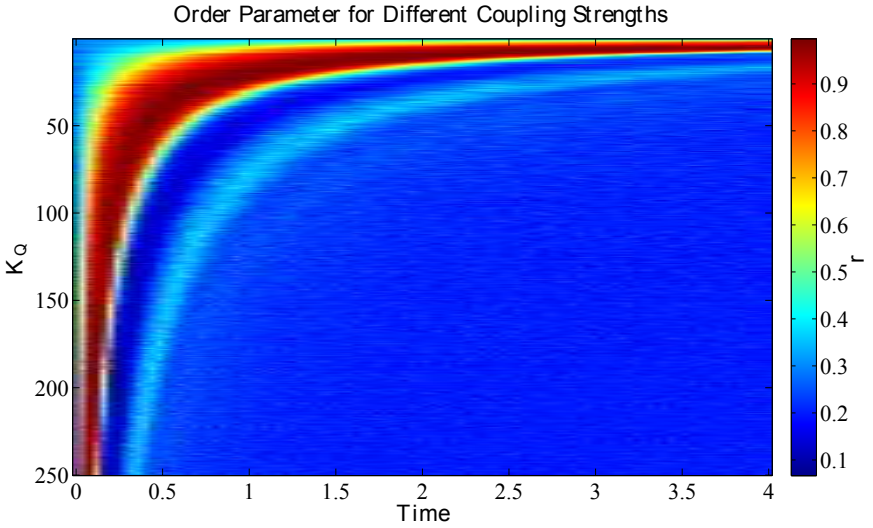

Figure 5.18: 10 modes, 100 samples with $\Delta\omega = 1$.

The first thing that I would like to show you is a scan across relatively high[7] values of K_Q (Figure 5.18). Here you can clearly see the inverse relation between T_s and K_Q; increasing K_Q causes the transient synchronization becomes shorter and shorter.

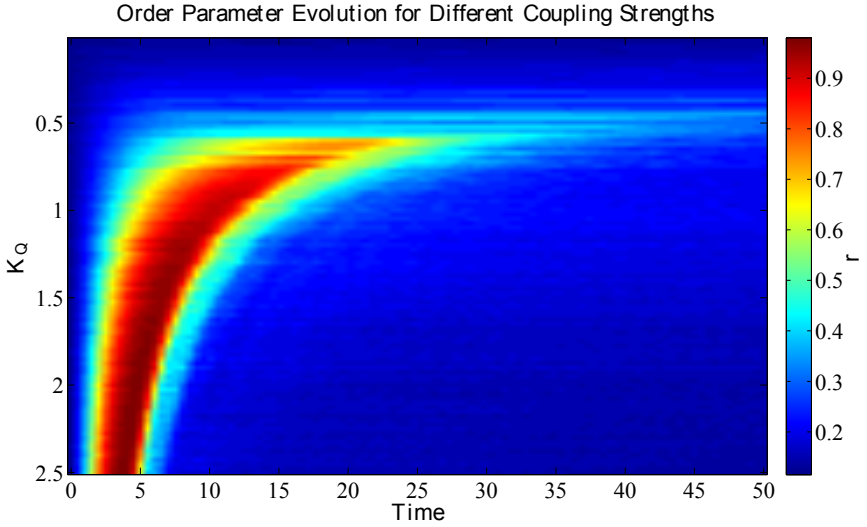

Figure 5.19: 50 modes, 100 samples with $\Delta\omega = 1$.

Figure 5.19 is a plot of lower values of K_Q where it is easy to see that there is a limit to how long T_s can be when varying only K_Q. This also shows that there is a phase transition between being able to have transient synchronization and not, analogous to figure 2.7.

Taking the maximum values of this plot across the y axis we produce figure 5.20. Here $(K_Q)_c$ is the classical limit critical coupling value found by comparing equations (5.12) and (2.10). Explicitly this is:

$$(K_Q)_c = \frac{2}{\pi g(0)} \tag{5.21}$$

Figure 5.20 shows that the phase transition occurs at the same place as it would in the classical limit. Simulations show that changing the number of bosons has the exact same effect as changing K_Q directly.

I did not find that changing the number of modes, while keeping n_{tot} constant, has an influence on anything but the level of noise in the system, with less modes producing noisier results.

[7]By relatively high I mean that the values are too high to see the phase transition, like in figure 5.19.

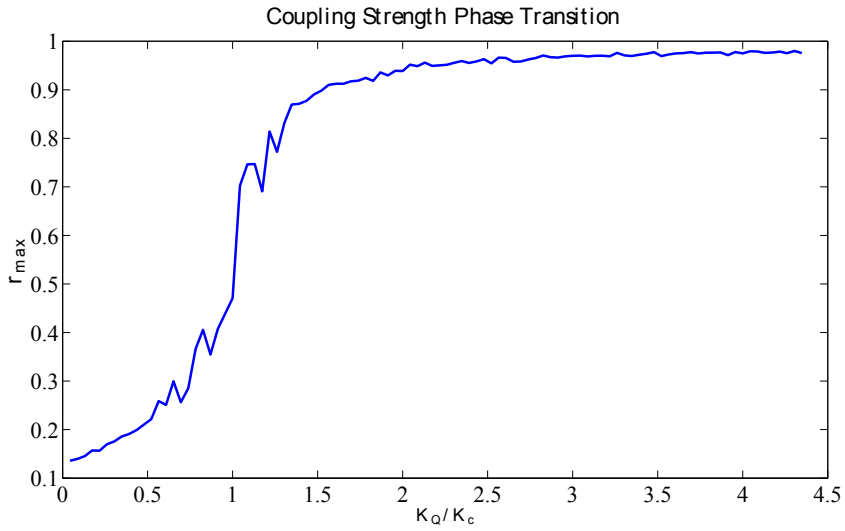

Figure 5.20: 20 modes, 300 samples with $\Delta\omega = 1$.

Chapter 6

Conclusion and Further Work

In this project I have successfully shown that there does exist a microscopic model that maps to Kuramoto when the appropriate limits are taken. I have analyzed the key aspects of said model's behaviour through the use of phase space methods and found that only transient synchronization is possible. This is what one would expect as Hamiltonian evolution is always time reversible.

The reason that the classical Kuramoto model is time irreversible is due to the fact that it is not a Hamiltonian description of the system. The behaviour is dissipative due to the form that the coupling takes[4].

There are several avenues of future work that I can see.

The first is in regards to the fact that I have been using the truncated Wigner method and discarded the third order terms when deriving my equations. A fortunate consequence of this was that I could scale my simulations down to a level that did not require much computation time. This was because, as appendix A.2 shows, the third order terms only come into play when the number or modes and bosons were low. So, with the truncated formalism, I could keep the same dynamics as the high number of modes and particles without them actually being high.

However this does raise the question of how the dynamics change with the third order terms included.

Another avenue that I would like to explore is in regards to reference [5]. What they have done is posed a different, more general way to define the level of synchronization in a quantum system. I would like to apply their methods to my model and see how they compare with my current results. This may have some interesting results for the trough depicted in figure 5.14 and shed light on why it exists. This paper came out while this dissertation was being written, so I didn't have time to act upon this.

Comparing my work with the papers [13, 14, 5, 15, 4], it seems that some form of external influence is required to achieve perpetual synchronization. In some of these cases it takes the form of external EM radiation. Indeed, in the Hamiltonian description of the Kuramoto Model[4] the system must be coupled to a large thermal bath of some description. Reference [4] works down from this classical Hamiltonian to construct their quantum Kuramoto analogy. Comparing my results with theirs would shed light on

what the conditions are required for our model to exhibit irreversible synchronization.

However, as their results came out 3 days before this dissertation was due I have not had time to investigate this.

The possibility of constructing a physical realization of our Hamiltonian is yet to be explored. I am very confident that it is possible to build such a system based on the versatility in current Hamiltonian construction methods. The level of sophistication in building coupled optical resonator arrays leads this to be a strong candidate, provided the coupling can be engineered with sufficient precision.

Finally, the field of quantum chaos introduces a way to scale the level of "quantumness" in a system.Applying this to our Hamiltonian would allow us to explore how our system transitions from classical regime into a quantum one. Hopefully one would observe some form of phase transition between irreversible and transient sync.

References

[1] A. Pikovsky, M. Rosenblum, and J. Kurths, "Synchronization: A universal concept in nonlinear science," *American Journal of Physics*, vol. Volume 70, Issue 6, p. pp. 655, June 2002.

[2] S. Strogatz, *Sync: the emerging science of spontaneous order*. 1st ed. ed., 2003.

[3] F. Marquardt and S. M. Girvin, "Optomechanics," *Physics*, vol. 2, p. 40, May 2009.

[4] I. H. de Mendoza, L. A. Pachn, J. Gmez-Gardees, and D. Zueco, "The quantum kuramoto model." September 2013.

[5] A. Mari, A. Farace, N. Dirdier, V. Giovannetti, and R. Fazio, "Measures of quantum synchronization in continuous variable systems," *Physical Review Letters*, September 2013.

[6] S. H. Strogatz, "From kuramoto to crawford: exploring the onset of synchronization in populations of coupled oscillators," *Physica D: Nonlinear Phenomena*, vol. 143, no. 14, pp. 1 – 20, 2000.

[7] "Firefly pictures."

[8] L. F. Abbott and C. van Vreeswijk, "Asynchronous states in networks of pulse-coupled oscillators," *Physical Review E*, vol. Vol. 48, No. 2., pp. pp. 1483–1490, 1 Aug 1993.

[9] C. S. Paskin, "Mathematical aspects of heart physiology," *[New York] Courant Institute of Mathematical Sciences, New York University*, pp. 268–278, 1975.

[10] R. E. Mirollo and S. H. Strogatz, "Synchronization of pulse-coupled biological oscillators," *SIAM Journal on Applied Mathematics*, vol. 50, no. 6, pp. 1645–1662, 1990.

[11] N. Weiner, "Nonlinear problems in random theory," *The MIT Press*, 1966.

[12] A. T. Winfree, *The Geometry of Biological Time*. Springer.

[13] G. Heinrich, M. Ludwig, J. Qian, B. Kubala, and F. Marquardt, "Collective dynamics in optomechanical arrays," *Phys. Rev. Lett.*, vol. 107, p. 043603, Jul 2011.

[14] C. A. Holmes, C. P. Meaney, and G. J. Milburn, "Synchronization of many nanomechanical resonators coupled via a common cavity field," *Phys. Rev. E*, vol. 85, p. 066203, Jun 2012.

[15] M. Xu, D. A. Tieri, E. C. Fine, J. K. Thompson, and M. J. Holland, "Quantum synchronization of two ensembles of atoms." July 2013.

[16] P. Z. C. W. Gardiner, *Quantum Noise*. Springer, third edition ed., 2004.

[17] "Gallery of wigner states."

[18] M. Olsen and A. Bradley, "Numerical representation of quantum states in the positive-p and wigner representations," *Optics Communications*, vol. 282, no. 19, pp. 3924 – 3929, 2009.

[19] P. Blakie, A. Bradley, M. Davis, R. Ballagh, and C. Gardiner, "Dynamics and statistical mechanics of ultra-cold Bose gases using c-field techniques," *Advances in Physics*, vol. 57, no. 5, pp. 372–384, 2008.

Appendices

A.1 Gaussian vs. Lorentzian

In section 2.2.1 I gave the solution for r_∞ for a Lorenztian frequency distribution, but said that I would be using Gaussian distributions in this dissertation. Here I will explain why this is.

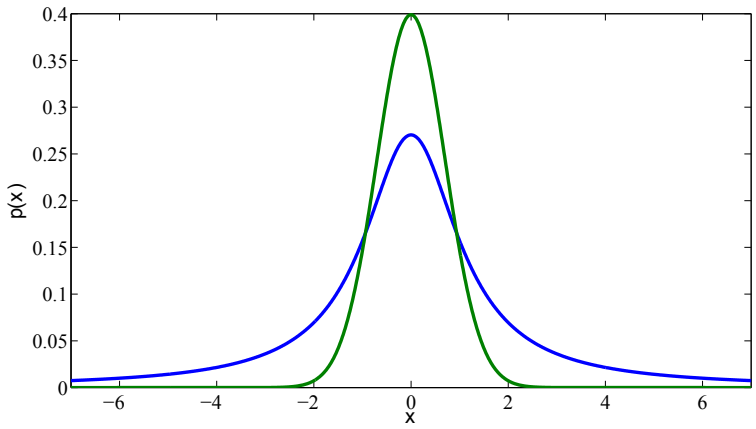

Figure A.1: A comparason of equal FWHM Lorentzian (blue) and Gaussian (green) distiributions.

A Lorentzian distribution is defined by the following equation:

$$L(x) = \frac{1}{\pi}\frac{\gamma}{x^2+\gamma^2} \tag{A.1}$$

and a gaussian distribution is defined:

$$G(x) = \frac{1}{\sqrt{2\pi}\sigma}\exp(\frac{-x^2}{2\sigma^2}) \tag{A.2}$$

In figure A.1 you can see that for similar width distributions, the Gaussian has a more centralized distribution than the Lorentzian. While in a continuous case this would not lead to any problems, a computer runs discrete simulations. When sampling points for say, frequency, one uses these probabillity distributions to generate a selection of numbers. From comparing figures A.2 and A.3, which both contain 10,000 randomly distributed numbers we finsd that the Gaussian distributes numbers more evenly. In

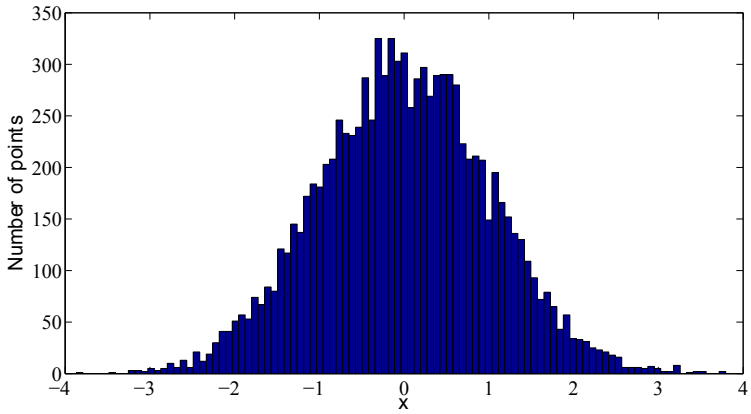

Figure A.2: A selection of 10,000 random Gaussian distributed points with FWHH=2.355

fact, the Lorentzian distribution will regularly make extreme outliers.

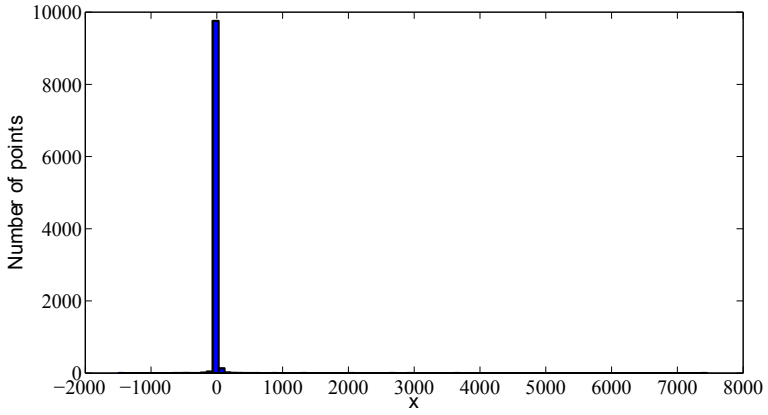

Figure A.3: A selection of 10,000 random Lorentzian distributed points with FWHH=2.355

If these were how the frequencies of oscillators then there would be a small distribution about a value, plodding along at a similar rate. But then there would be a few zipping around, thousands of times the speed of the rest. Since the Kuramoto model deals with similar oscillators I have decided to use Gaussian distributions for all of my

needs.

A.2 Deriving the Phase Space Equations

For a density operator ρ the converting to the Wigner formulation has the following rules:

$$a\rho \leftrightarrow (\alpha + \frac{1}{2}\frac{\partial}{\partial\bar{\alpha}})W(\boldsymbol{\alpha},\boldsymbol{\alpha^*}) \tag{A.3a}$$

$$a^\dagger\rho \leftrightarrow (\bar{\alpha} - \frac{1}{2}\frac{\partial}{\partial\alpha})W(\boldsymbol{\alpha},\boldsymbol{\alpha^*}) \tag{A.3b}$$

$$\rho a \leftrightarrow (\alpha - \frac{1}{2}\frac{\partial}{\partial\bar{\alpha}})W(\boldsymbol{\alpha},\boldsymbol{\alpha^*}) \tag{A.3c}$$

$$\rho a^\dagger \leftrightarrow (\bar{\alpha} + \frac{1}{2}\frac{\partial}{\partial\alpha})W(\boldsymbol{\alpha},\boldsymbol{\alpha^*}) \tag{A.3d}$$

The time evolution of the density operator is:

$$\begin{aligned}\frac{\partial\rho}{\partial t} &= -\frac{i}{\hbar}[H,\rho] \\ &= -i\sum_j \omega_j(a_j^\dagger a_j\rho - \rho a_j^\dagger a_j) + \sum_{<j,k>}\chi_{jk}(a_j^\dagger a_j a_k^\dagger a_j\rho - \rho a_j^\dagger a_j a_k^\dagger a_j - a_j^\dagger a_k a_j^\dagger a_j\rho + \rho a_j^\dagger a_k a_j^\dagger a_j)\end{aligned} \tag{A.4}$$

This is the Wigner fromulation is quite long, so we will break it up into sections. Denoting the partial derivative with restpect to α_j as ∂_{α_j}, the single mode part gives:

$$\begin{aligned}-i\sum_j \omega_j(a_j^\dagger a_j\rho - \rho a_j^\dagger a_j) &\leftrightarrow -i\sum_j \omega_j\left[(\alpha_j^* - \tfrac{1}{2}\partial_{\alpha_j})(\alpha_j + \tfrac{1}{2}\partial_{\alpha_j^*}) - (\alpha_j - \tfrac{1}{2}\partial_{\alpha_j^*})(\alpha_j^* + \tfrac{1}{2}\partial_{\alpha_j})\right]W(\boldsymbol{\alpha},\boldsymbol{\alpha^*}) \\ &= -\frac{i}{2}\sum_j \omega_j\left(\alpha_j^*\partial_{\alpha_j^*} - \partial_{\alpha_j}\alpha_j - \alpha_j\partial_{\alpha_j} + \partial_{\alpha_j^*}\alpha_j^*\right)W(\boldsymbol{\alpha},\boldsymbol{\alpha^*}) \\ &= -\sum_j\left(\partial_{\alpha_j^*}(i\omega_j\alpha_j^*) + \partial_{\alpha_j}(-i\omega_j\alpha_j)\right)W(\boldsymbol{\alpha},\boldsymbol{\alpha^*})\end{aligned} \tag{A.5}$$

The first double sum commutator gives:

$$\begin{aligned}\sum_{<j,k>}\chi_{jk}(a_j^\dagger a_j a_k^\dagger a_j\rho - \rho a_j^\dagger a_j a_k^\dagger a_j) \leftrightarrow \sum_{<j,k>}\chi_{jk}\big[&(\alpha_j^* - \tfrac{1}{2}\partial_{\alpha_j})(\alpha_j + \tfrac{1}{2}\partial_{\alpha_j^*})(\alpha_k^* - \tfrac{1}{2}\partial_{\alpha_k})(\alpha_j + \tfrac{1}{2}\partial_{\alpha_j^*}) \\ &- (\alpha_j - \tfrac{1}{2}\partial_{\alpha_j^*})(\alpha_k^* + \tfrac{1}{2}\partial_{\alpha_k})(\alpha_j - \tfrac{1}{2}\partial_{\alpha_j^*})(\alpha_j^* + \tfrac{1}{2}\partial_{\alpha_j})\big]W(\boldsymbol{\alpha},\boldsymbol{\alpha^*})\end{aligned} \tag{A.6}$$

It is easy to see that the 0th and 4th order terms cancel, so the 1st order terms are:

$$\begin{aligned}\tfrac{1}{2}(&\alpha_j^*\alpha_j\alpha_k^*\partial_{\alpha_j^*} - \alpha_j^*\alpha_j\partial_{\alpha_k}\alpha_j + \alpha_j^*\partial_{\alpha_j^*}\alpha_k^*\alpha_j - \partial_{\alpha_j}\alpha_j\alpha_k^*\alpha_j - \alpha_j\alpha_k^*\alpha_j\partial_{\alpha_j} + \alpha_j\alpha_k^*\partial_{\alpha_j^*}\alpha_j^* - \alpha_j\partial_{\alpha_k}\alpha_j\alpha_j^* + \partial_{\alpha_j^*}\alpha_k^*\alpha_j\\ &=(2\partial_{\alpha_j^*}\alpha_j^*\alpha_k^*\alpha_j - \partial_{\alpha_k}\alpha_j^*\alpha_j\alpha_j - \partial_{\alpha_j}\alpha_k^*\alpha_j\alpha_j)W(\boldsymbol{\alpha},\boldsymbol{\alpha^*}) \qquad \text{(A.7)}\end{aligned}$$

2nd order:

$$\begin{aligned}\tfrac{1}{4}(&-\alpha_j^*\alpha_j\partial_{\alpha_k}\partial_{\alpha_j^*} - \alpha_j^*\partial_{\alpha_j^*}\partial_{\alpha_k}\alpha_j + \alpha_j\partial_{\alpha_k}\partial_{\alpha_j^*}\alpha_j^* + \partial_{\alpha_j^*}\partial_{\alpha_k}\alpha_j\alpha_j^* + \alpha_j^*\partial_{\alpha_j^*}\alpha_k^*\partial_{\alpha_j^*} - \partial_{\alpha_j^*}\alpha_k^*\partial_{\alpha_j^*}\alpha_j^*\\ &+\partial_{\alpha_j}\alpha_j\partial_{\alpha_k}\alpha_j - \alpha_j\partial_{\alpha_k}\alpha_j\partial_{\alpha_j} - \partial_{\alpha_j}\alpha_j\alpha_k^*\partial_{\alpha_j^*} - \partial_{\alpha_j}\partial_{\alpha_j^*}\alpha_k^*\alpha_j + \alpha_j\alpha_k^*\partial_{\alpha_j^*}\partial_{\alpha_j} + \partial_{\alpha_j^*}\alpha_k^*\alpha_j\partial_{\alpha_j})W(\boldsymbol{\alpha},\boldsymbol{\alpha^*})\\ &=\tfrac{1}{2}(\partial_{\alpha_k}\alpha_j + \partial_{\alpha_j^*}\alpha_k^* - \partial_{\alpha_k}\alpha_j - \partial_{\alpha_j^*}\alpha_k^*)W(\boldsymbol{\alpha},\boldsymbol{\alpha^*})\\ &=0 \qquad \text{(A.8)}\end{aligned}$$

3rd order:

$$\begin{aligned}\tfrac{1}{8}(&-\alpha_j^*\partial_{\alpha_j^*}\partial_{\alpha_k}\partial_{\alpha_j^*} + \partial_{\alpha_j}\alpha_j\partial_{\alpha_k}\partial_{\alpha_j^*} - \partial_{\alpha_j}\partial_{\alpha_j^*}\alpha_k^*\partial_{\alpha_j^*} + \partial_{\alpha_j}\partial_{\alpha_j^*}\partial_{\alpha_k}\alpha_j - \alpha_j\partial_{\alpha_k}\partial_{\alpha_j^*}\partial_{\alpha_j}\\ &+\partial_{\alpha_j^*}\alpha_k^*\partial_{\alpha_j^*}\partial_{\alpha_j} - \partial_{\alpha_j^*}\partial_{\alpha_k}\alpha_j\partial_{\alpha_j} + \partial_{\alpha_j^*}\partial_{\alpha_k}\partial_{\alpha_j^*}\alpha_j^*)W(\boldsymbol{\alpha},\boldsymbol{\alpha^*})\\ &=\tfrac{1}{4}(2\partial_{\alpha_j^*}\partial_{\alpha_j}\partial_{\alpha_k}\alpha_j - \partial_{\alpha_j^*}\partial_{\alpha_j^*}\partial_{\alpha_k}\alpha_j^* - \partial_{\alpha_j^*}\partial_{\alpha_j^*}\partial_{\alpha_j}\alpha_k^*)W(\boldsymbol{\alpha},\boldsymbol{\alpha^*}) \qquad \text{(A.9)}\end{aligned}$$

Repeating this for the remaining terms:

$$\begin{aligned}-\sum_{<j,k>}\chi_{jk}(a_j^\dagger a_k a_j^\dagger a_j\rho - \rho a_j^\dagger a_k a_j^\dagger a_j) \leftrightarrow -\sum_{<j,k>}\chi_{jk}\big[&(\alpha_j^* - \tfrac{1}{2}\partial_{\alpha_j})(\alpha_k + \tfrac{1}{2}\partial_{\alpha_k^*})(\alpha_j^* - \tfrac{1}{2}\partial_{\alpha_j})(\alpha_j + \tfrac{1}{2}\partial_{\alpha_j^*})\\ &-(\alpha_j - \tfrac{1}{2}\partial_{\alpha_j^*})(\alpha_j^* + \tfrac{1}{2}\partial_{\alpha_j})(\alpha_k - \tfrac{1}{2}\partial_{\alpha_k^*})(\alpha_j^* + \tfrac{1}{2}\partial_{\alpha_j})\big]W(\boldsymbol{\alpha},\boldsymbol{\alpha^*})\end{aligned} \qquad \text{(A.10)}$$

1st order:

$$\begin{aligned}-\tfrac{1}{2}(&\alpha_j^*\alpha_k\alpha_j^*\partial_{\alpha_j^*} - \alpha_j^*\alpha_k\partial_{\alpha_j}\alpha_j + \alpha_j^*\partial_{\alpha_k^*}\alpha_j^*\alpha_j - \partial_{\alpha_j}\alpha_k\alpha_j^*\alpha_j - \alpha_j\alpha_j^*\alpha_k\partial_{\alpha_j} + \alpha_j\alpha_j^*\partial_{\alpha_k^*}\alpha_j^* - \alpha_j\partial_{\alpha_j}\alpha_k\alpha_j^* + \partial_{\alpha_j^*}\alpha_j^*\\ &=(2\partial_{\alpha_j}\alpha_j^*\alpha_j\alpha_k - \partial_{\alpha_k^*}\alpha_j^*\alpha_j^*\alpha_j - \partial_{\alpha_j^*}\alpha_k^*\alpha_j^*\alpha_k)W(\boldsymbol{\alpha},\boldsymbol{\alpha^*}) \qquad \text{(A.11)}\end{aligned}$$

2nd order:

$$\begin{aligned}-\tfrac{1}{4}(&-\alpha_j^*\alpha_k\partial_{\alpha_j}\partial_{\alpha_j^*} - \alpha_j^*\partial_{\alpha_k^*}\partial_{\alpha_j}\alpha_j + \alpha_j\partial_{\alpha_j}\partial_{\alpha_k^*}\alpha_j^* + \partial_{\alpha_j^*}\partial_{\alpha_j}\alpha_k\alpha_j^* + \alpha_j^*\partial_{\alpha_k^*}\alpha_j^*\partial_{\alpha_j^*} - \partial_{\alpha_j^*}\alpha_j^*\partial_{\alpha_k^*}\alpha_j^*\\ &+\partial_{\alpha_j}\alpha_k\partial_{\alpha_j}\alpha_j - \alpha_j\partial_{\alpha_j}\alpha_k\partial_{\alpha_j} - \partial_{\alpha_j}\alpha_j\alpha_k^*\partial_{\alpha_j^*} - \partial_{\alpha_j}\partial_{\alpha_k^*}\alpha_j^*\alpha_j + \alpha_j\alpha_j^*\partial_{\alpha_k^*}\partial_{\alpha_j} + \partial_{\alpha_j^*}\alpha_j^*\alpha_k\partial_{\alpha_j})W(\boldsymbol{\alpha},\boldsymbol{\alpha^*})\\ &=-\tfrac{1}{2}(\partial_{\alpha_k^*}\alpha_j^* + \partial_{\alpha_j}\alpha_k - \partial_{\alpha_k^*}\alpha_j^* - \partial_{\alpha_j}\alpha_k)W(\boldsymbol{\alpha},\boldsymbol{\alpha^*})\\ &=0 \qquad \text{(A.12)}\end{aligned}$$

3rd order:

$$\begin{aligned}
&\tfrac{1}{8}\big(- \alpha_j^*\partial_{\alpha_k^*}\partial_{\alpha_j}\partial_{\alpha_j^*} + \partial_{\alpha_j}\alpha_k\partial_{\alpha_j}\partial_{\alpha_j^*} - \partial_{\alpha_j}\partial_{\alpha_k^*}\alpha_j^*\partial_{\alpha_j^*} + \partial_{\alpha_j}\partial_{\alpha_k^*}\partial_{\alpha_j}\alpha_j - \alpha_j\partial_{\alpha_j}\partial_{\alpha_k^*}\partial_{\alpha_j} \\
&\quad + \partial_{\alpha_j^*}\alpha_j^*\partial_{\alpha_k^*}\partial_{\alpha_j} - \partial_{\alpha_j^*}\partial_{\alpha_j}\alpha_k\partial_{\alpha_j} + \partial_{\alpha_j^*}\partial_{\alpha_j}\partial_{\alpha_k^*}\alpha_j^*)W(\boldsymbol{\alpha},\boldsymbol{\alpha^*}) \\
&= \tfrac{1}{4}(2\partial_{\alpha_j^*}\partial_{\alpha_k^*}\partial_{\alpha_j}\alpha_j^* - \partial_{\alpha_k^*}\partial_{\alpha_j}\partial_{\alpha_j}\alpha_j - \partial_{\alpha_j^*}\partial_{\alpha_j}\partial_{\alpha_j}\alpha_k)W(\boldsymbol{\alpha},\boldsymbol{\alpha^*}) \qquad \text{(A.13)}
\end{aligned}$$

Combining all of these we have:

$$\begin{aligned}
\frac{\partial W}{\partial t} &= \left(\frac{\partial W}{\partial t}\right)_{1st} + \left(\frac{\partial W}{\partial t}\right)_{3rd} \\
&= \left(\frac{\partial W}{\partial t}\right)_{SM} + \left(\frac{\partial W}{\partial t}\right)_{Int} + \left(\frac{\partial W}{\partial t}\right)_{3rd} \qquad \text{(A.14)}
\end{aligned}$$

where,

$$\left(\frac{\partial W}{\partial t}\right)_{SM} = -\sum_j \Big[\partial_{\alpha_j^*}(i\omega_j\alpha_j^*) + \partial_{\alpha_j}(-i\omega_j\alpha_j)\Big]\, W(\alpha,\bar{\alpha}), \qquad \text{(A.15)}$$

$$\begin{aligned}
\left(\frac{\partial W}{\partial t}\right)_{Int} &= -\sum_{<j,k>}\Big[\big(\partial_{\alpha_j}(\chi_{jk}\alpha_k^*\alpha_j\alpha_j - 2\chi_{jk}\alpha_j^*\alpha_j\alpha_k) + \partial_{\alpha_k}(\chi_{jk}\alpha_j^*\alpha_j\alpha_j)\big) + c.c.\Big]W(\boldsymbol{\alpha},\boldsymbol{\alpha^*}) \\
&= -\sum_j\Big[\partial_{\alpha_j}\big(\sum_{k\neq j}\chi_{jk}(\alpha_k^*\alpha_j\alpha_j - 2\alpha_j^*\alpha_j\alpha_k + \alpha_k^*\alpha_k\alpha_k)\big) + c.c.\Big]W(\boldsymbol{\alpha},\boldsymbol{\alpha^*}), \\
&\qquad \text{(A.16)}
\end{aligned}$$

and

$$\left(\frac{\partial W}{\partial t}\right)_{3rd} = -\sum_{<j,k>}\Big[\big(\partial_{\alpha_j^*}\partial_{\alpha_j}\partial_{\alpha_j}(\tfrac{1}{4}\chi_{jk}\alpha_k) + \partial_{\alpha_k^*}\partial_{\alpha_j}\partial_{\alpha_j}(\tfrac{1}{4}\chi_{jk}\alpha_j) - \partial_{\alpha_j^*}\partial_{\alpha_j}\partial_{\alpha_k}(\tfrac{1}{2}\chi_{jk}\alpha_j)\big) + c.c.\Big]W(\boldsymbol{\alpha},\boldsymbol{\alpha^*}) \qquad \text{(A.17)}$$

Let's take a look at the classical limit. Take $\alpha_j = \sqrt{n_j}\tilde{\alpha_j}$, then let let $\chi_{jk} \to 0$ and $n_j \to \infty$ for all j,k such that $n_j\chi_{jk} = const.$
The first order terms are essentially unchanged as,

$$\begin{aligned}
&\partial_{\alpha_j}\Big(- i\omega_j\alpha_j + \sum_{k\neq j}\chi_{jk}(\alpha_k^*\alpha_j\alpha_j - 2\alpha_j^*\alpha_j\alpha_k + \alpha_k^*\alpha_k\alpha_k)\Big) \\
&\qquad = \frac{\partial_{\tilde{\alpha_j}}}{\sqrt{n_j}}\Big(- i\sqrt{n_j}\omega_j\tilde{\alpha_j} + \sum_{k\neq j}\chi_{jk}(n_j\sqrt{n_k}\tilde{\alpha_k}^*\tilde{\alpha_j}\tilde{\alpha_j} - n_j\sqrt{n_k}2\tilde{\alpha_j}^*\tilde{\alpha_j}\tilde{\alpha_k} + (n_k)^{\frac{3}{2}}\tilde{\alpha_k}^*\tilde{\alpha_k}\tilde{\alpha_k})\Big) \\
&\qquad \to \partial_{\tilde{\alpha_j}}\Big(- i\omega_j\tilde{\alpha_j} + \sum_{k\neq j}\chi_{jk}(\tilde{\alpha_k}^*\tilde{\alpha_j}\tilde{\alpha_j} - 2\tilde{\alpha_j}^*\tilde{\alpha_j}\tilde{\alpha_k} + \tilde{\alpha_k}^*\tilde{\alpha_k}\tilde{\alpha_k})\Big)
\end{aligned}$$

But the third order terms vanish:

$$\begin{aligned}\chi_{jk}\partial_{\alpha_j^*}\partial_{\alpha_j}\partial_{\alpha_j}(\tfrac{1}{4}\alpha_k) + \partial_{\alpha_k^*}\partial_{\alpha_j}\partial_{\alpha_j}(\tfrac{1}{4}\alpha_j) - \partial_{\alpha_j^*}\partial_{\alpha_j}\partial_{\alpha_k}(\tfrac{1}{2}\alpha_j)& \\ = \frac{\chi_{jk}}{n_j}\big[\sqrt{\frac{n_k}{n_j}}\partial_{\tilde{\alpha_j^*}}\partial_{\tilde{\alpha_j}}\partial_{\tilde{\alpha_j}}(\tfrac{1}{4}\tilde{\alpha_k}) + \sqrt{\frac{n_j}{n_k}}\partial_{\tilde{\alpha_k^*}}\partial_{\tilde{\alpha_j}}\partial_{\tilde{\alpha_j}}(\tfrac{1}{4}\tilde{\alpha_j}) - \sqrt{\frac{n_j}{n_k}}\partial_{\tilde{\alpha_j^*}}\partial_{\tilde{\alpha_j}}\partial_{\tilde{\alpha_k}}(\tfrac{1}{2}\tilde{\alpha_j})\big]& \\ \to 0&\end{aligned}$$

Hence it is an apropriate approximation to use the Truncated Wigner Fromulation, that is; to ignore the Third order terms. Without the third order terms we have:

$$\begin{aligned}\frac{\partial W(\boldsymbol{\alpha},\boldsymbol{\alpha^*})}{\partial t} &\approx -\sum_j \partial_{\alpha_j}\big(-i\omega_j\alpha_j + \sum_{k\neq j}\chi_{jk}(\alpha_k^*\alpha_j\alpha_j - 2\alpha_j^*\alpha_j\alpha_k + \alpha_k^*\alpha_k\alpha_k)\big) + c.c.\Big]W(\boldsymbol{\alpha},\boldsymbol{\alpha^*}) \\ &= -\sum_j\left[\partial_{\alpha_j}\left(-\frac{i}{\hbar}\frac{\partial H(\boldsymbol{\alpha},\boldsymbol{\alpha^*})}{\partial\alpha_j^*}\right) + c.c\right]W(\boldsymbol{\alpha},\boldsymbol{\alpha^*}) \qquad \text{(A.18)}\end{aligned}$$

This yeilds the equations of motion:

$$d\alpha_j = -\frac{i}{\hbar}\frac{\partial H(\boldsymbol{\alpha},\boldsymbol{\alpha^*})}{\partial\alpha_j^*}dt \qquad \text{(A.19)}$$

Because there were not any second order terms, there are no diffusion terms in equation and hence there is no explicit noise. However the initial conditions are stochastic will need to be sampled apropriately (see 4.0.2).